UNIVERSITY OF THESSALY
DEPARTMENT OF MECHANICAL ENGINEERING
LABORATORY OF MATERIALS

Thermodynamic and Kinetic Analysis of Nitriding in Ductile Cast Iron

Fe- 3.4%C- 4%Si- 1%Nb- (0-4) %Al

BY:

MYRTO ROUTSI

THESIS SUPERVISOR:

HELEN KAMOUTSI

PROFESSOR OF PHYSICAL METALLURGY

UNIVERSITY OF THESSALY

Members of the Examining Committee:

Thesis Supervisor: Dr. Helen Kamoutsi
Laboratory Teaching Staff
Department of Mechanical Engineering
University of Thessaly

Second Examiner: Dr. Gregory Haidemenopoulos
Professor of Physical Metallurgy
Department of Mechanical Engineering
University of Thessaly

Third Examiner: Dr. Alexis Kermanidis
Associate Professor of Mechanical Behavior of Materials
Department of Mechanical Engineering
University of Thessaly

Table of Contents

TABLE OF FIGURES

CHAPTER 2.1

CHAPTER 2.2

CHAPTER 3.1

CHAPTER 3.2

CHAPTER 4.2

CHAPTER 4.3

CHAPTER 4.4

CHAPTER 4.5

CHAPTER 4.6

TABLES

ABSTRACT

The subject of this thesis is the calculation and analysis of the thermodynamic data and kinetic simulations in ductile cast iron Fe-3.4wt%C-4wt%Si-1wt%Nb-(0-4) wt%Al in order to study and predict the surface's final form and properties. The goal of the nitriding heat treatment is to enhance surface hardness, fatigue strength, wear and corrosion resistance, improving efficiency and longevity of cast iron components used in demanding conditions. THERMOCALC software is used to calculate phase diagrams, phase fractions and ferritic phase compositions for the cast iron, for different Al contents. It is observed that the suspension of Si_3N_4 phase leads to the formation of γ'-nitrides for lower nitrogen percentages, as well as the formation of ε-nitrides in higher amounts. The addition of aluminum introduces kappa phase rich in Al and increases the Nwt% ranges that γ' is formed. Afterwards, based on the thermodynamic data, kinetic simulations for a small region at the beginning of the surface's diffusion zone are performed, using DICTRA software. The effect of nitrogen activity, nitriding temperature and Si content on the nitrogen diffusion, γ'-nitride formation and region distance penetration is examined at different times. For activity value 100, the simulation results exhibit numerical instabilities, however with the increase of the activity to 1000 those results are more stable and gradual, resulting in deeper insertion of N and γ' into the region. Even bigger activity increase to 3000 results in diffusion of higher nitrogen percentages, and creation of thicker nitride layer. Next, the simulation of a 10◦C nitriding temperature increase results in more stable calculations for lower nitrogen activity, decrease of γ'-nitride formation at the same distance for medium activity, as well as the formation of thicker nitride layer deeper into the diffusion zone, however not as rich in γ'-nitrides.

This thesis contributes to the understanding of the thermodynamic and kinetic processes involved in ferritic ductile cast iron nitriding, providing valuable insights for industrial applications where enhanced surface hardness and durability are essential. Some of these applications are engine components like crankshafts, gears, valve stems, transmission systems in the automotive industry, steam and gas turbines for power generation, pipelines, valves, connectors and fitting in the oil and gas industry and finally, mining and construction equipment for heavy machinery, all requiring resistance to withstand abrasive environments.

CHAPTER 1: Introduction

1.1 Ductile Cast Irons

Ductile cast iron is a commonly used metal substance that contains 3.0-4.0wt% of carbon component. Due to its properties, this material is often highly preferred in industrial production and has many applications in various industries. Characterized by high strength and durability, ductile cast iron is often the optimal choice in engine component manufacture, while its great fatigue strength, wear performance and corrosion resistance make it suitable for production of water pipes, valves and connecting rods used in demanding conditions, such as saltwater, humidity or chemical exposure, for an extended period of time. This type of cast iron is distinguished by its microstructure, containing spheroidal nodules of graphite evenly distributed through the ferrous matrix in such a way, that those nodules work as obstacles against crack propagation leading to fracture, while at the same time making the material able to withstand significant elongation and plastic deformation. Ductility is considered to be this material's most important advantage and sets it apart from other types of cast iron, providing it with great malleability in production processing, as well as an impressive lifespan. Ductile cast iron is also widely referred as nodular or spheroidal graphite iron due to its uniform microstructure which can have a ferritic, pearlitic, bainitic or martensitic matrix depending on factors such as alloy composition, heat treatment and cooling process. Best ductility is evident in irons of ferritic matrix structure since the ferritic phase exhibits more stability up to 600 °C **[1].**

There are various cases that require the use of cast iron components in high temperatures. In exhaust manifolds of internal combustion engines in the automotive industry, the temperature can rise up to 1000°C due to hot exhaust gas flow. This can lead to material oxidation after continuous use as well as mechanical and thermal wear due to stresses. It is therefore very important to use a material that has the ability to withstand these kinds of conditions while at the same time have a low cost in order to be used frequently in the production industry.

In order to successfully create the desired surface texture characterized by hardness, durability and wear resistance, the heat-treating process of nitriding is widely used in industrial settings. Nitriding takes place inside furnaces consisting of a nitriding medium of ammonia (NH_3) which can be in the form of gas, salt, or plasma. During the treatment occurs the diffusion of nitrogen atoms inside the cast iron's lattice, forming two surface layers, the Compound Layer and the Diffusion Zone. At the end of the process, surface hardness and resistance are attributed to these two zones. The final surface microstructure is affected by parameters such as treatment duration, nitriding temperature, medium composition, as well as alloying elements' contents.

1.2 Thesis Subject

Due to the above, it is greatly important for the manufacturing industry to be able to use the nitriding process in a controlled way in order to be led to specific, predictable results when it comes to material surface texture and properties. Therefore, the goals of this thesis are:

- The understanding of the nitriding mechanism and process by gathering information from previous experimental studies and papers.

- Calculations of thermodynamic data, phase diagrams, phase fractions as well as compositions of alloying elements inside the ferritic lattice of a ferritic ductile cast iron.

- The study of the effect of aluminum (Al) addition to the alloying system.

- The kinetic simulation of the nitriding process of the ferritic ductile cast iron at nitriding temperature of 510◦C, which leads to the ability to analyze and predict nitrogen concentration caused by the diffusion, as well as the content of phases at the final microstructure.

CHAPTER 2: Nitriding- Literature Review

2.1 Nitriding Process

Surface Engineering is a term used to describe the final stage of processing of a material in order to adjust and enhance the microstructure and mechanical properties of its surface. Heat treatment constitutes one of the most important types of surface engineering that provides hardening of the outer surface of a material while maintaining its inner ductile properties. This type of materials is crucial in applications that require strength, wear and friction resistance while also being durable and not easily fractured. The main idea of thermochemical treatments is to enrich the material's surface layer in one of the alloying elements through the process of high temperature diffusion. The alloying elements that are most commonly increased in amount are carbon [C] or/and nitrogen [N], and these treatments are known as carburizing, nitriding or nitrocarburizing as the combination of the two. Nitriding can be applied to all types of steel and cast iron without any restriction.

Nitriding industrial process can occur in various forms. The most commonly used base conditions are gas, salt bath and plasma. A gaseous medium is oftentimes optimal, and is preferred in the industry, due to the easily controlled and manipulated gas conditions and composition, as well as control of basic thermodynamic parameters. Nitriding treatment is performed in specially designed annealing furnaces containing NH_3 in gaseous form, where nitrogen is diffused into iron surface at a temperature ranging from 480-550◦C. At these temperatures the microstructure of the iron consists of α-ferritic phase. The iron material undergoes the nitriding process in the furnace for approximately 20-80 hours **[2]**.

During nitriding, diffusion of N atoms occurs into the surface of the treated material, separating it into two different zones. The Compound Layer, rich in hard Fe nitrides (γ', ε), creating a strong, complex outer surface that exhibits great anti-wear and anti-corrosion properties, as well as the ferritic-based Diffusion Zone, that exists in greater depth of the surface, consists of dispersed N-phases and contributes greatly to the materials high fatigue resistance and durability. The increased surface hardness of the material is attributed to the following factors:

- The thick and detailed dispersion of small-sized nitrides.
- High dislocation density into the atomic lattice.
- Solid solution strengthening due to the high concentration of Nitrogen in interstitial positions within the ferritic lattice.
- Presence of other alloying elements, such as Al, Cr, Nb, V that, through formation of their own hard nitrides, offer added hardness to the surface.

The following figure *[Figure 2.1. 1]* presents a schematic image of the structure of the 2 nitriding zones of the nitrided material's surface, in relation to the surface's hardness.

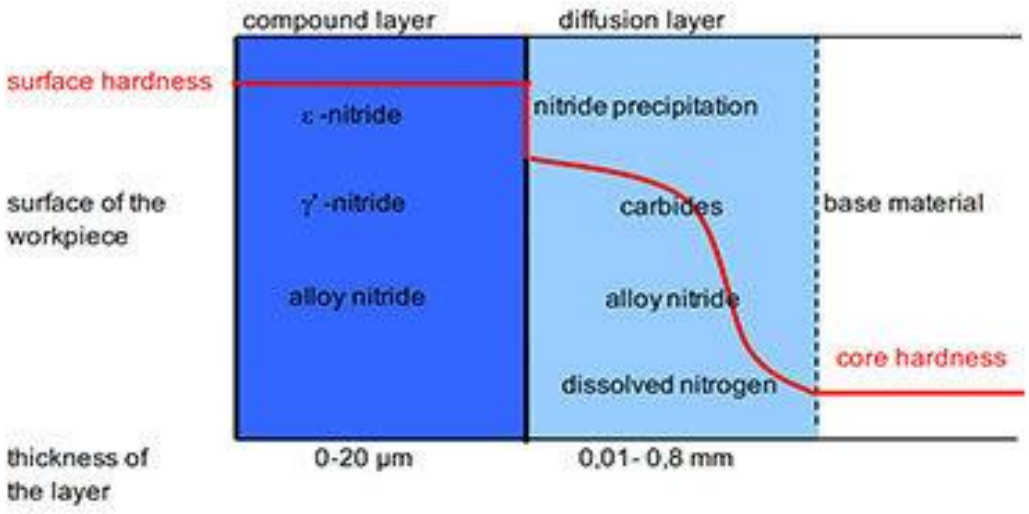

Figure 2.1. 1: Schematic of compound layer and diffusion zone structure and hardness

There was a study conducted by Kondakci and Solak at Istanbul's Technical University [3] with the goal of exploring the effect of microstructure on nitriding mechanism of cast iron. *Figure 2.1. 2* shows the initial microstructure of the 3 samples that were used for this research, as shown through SEM (Scanning Electron Microscopy) examination. The compositions (wt%) of the samples were the following:

a) EN-GJS-500: Fe-3.65C-2.55Si-0.22Mn-0.05Mg-0.32Cu-0.01S
b) EN-GJV-450: Fe-3.76C-2.22Si-0.24Mn-0.0084Mg-0.82Cu-0.012S
c) EN-GJL-250: Fe-3.25C-2.56Si-0.56Mn-0.12Cu-0.054S

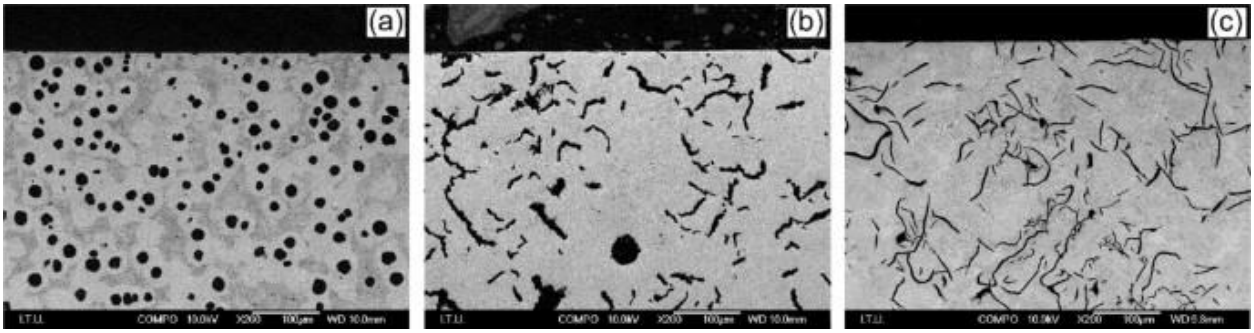

Figure 2.1. 2: SEM images of un-nitrided samples: (a) EN-GJS-500, (b) EN-GJV-450, (c) EN-GJL-250 [3]

Firstly, the samples were machined and polished in order to create a smooth surface on which the final heat treatment (nitriding) would take place. Afterwards the samples were placed in nitrogen atmosphere where they got heated at rate 10◦C/min, then the gas-nitriding process occurred at 525◦C in ammonia environment and finally the cast irons were cooled down inside the furnace. The examination after the end of the whole process was made through X-ray mapping, and the results can be shown in ***Figure 2.1. 3***, where the N atoms diffused into the samples' microstructure are visible and represented by red dots. These results offer the following conclusions **[4]** concerning the effect of microstructure on nitriding process:

- There are 3 distinct paths that nitrogen atoms follow during their diffusion in cast iron surface. They are inserted into the grains, they follow the grain boundaries, or graphite boundaries.
- The concentration of nitrogen appears higher along the grain boundaries and graphite particle boundaries (great number of red dots), so it is assumed that these are the paths that the N atoms mostly follow.
- It is therefore concluded that, along those primary paths, nitrogen diffusion has lower activation energy than on the inside of the grains.

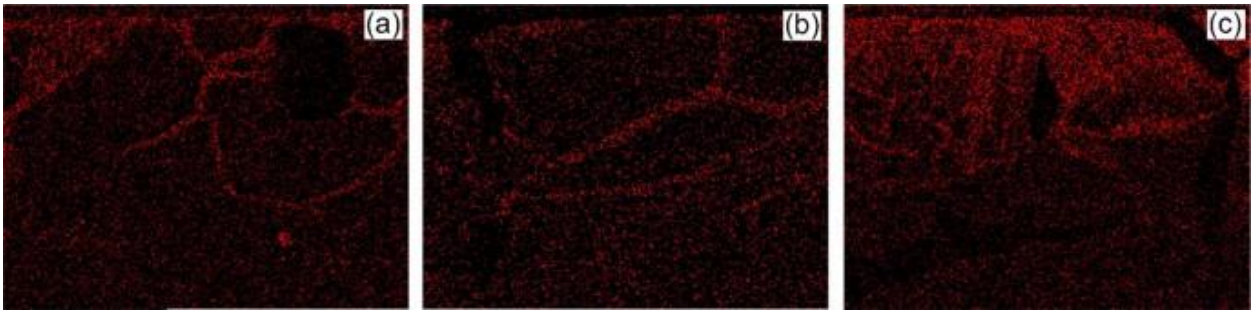

Figure 2.1. 3: X-ray mapping results of nitrided cast-iron samples. Red dots indicate nitrogen atoms: (a) EN-GJS500, (b) EN-GJV-450, (c) EN-GJL-250 **[3]**

In a different study Du, Somers and Agren investigated the influence of the composition of gas mixture (N and C activities) on the microstructural evolution and growth kinetics of the compound layer formed during gaseous nitrocarburizing of iron and iron-carbon samples at 575◦C. In each case that was examined it was noticed that the first step in the development of the compound layer of the specimens' surface was the nucleation of cementite. The fact that ammonia NH_3 dissociates in a slow pace combined with the fast reduction of CO by H_2 at the sample surface is what causes the cementite development prior to the nucleation of a (carbo)nitride phase. The investigation of growth kinetics also revealed that compound layers consisting of mostly one phase ε-Fe_2(N, C) develop the fastest, while the formation and growth of phase γ'-Fe_4(N, C) that occurs later at the interface of the compound layer and diffusion zone leads to delayed kinetics development. The study resulted in the understanding that due to lack of thermodynamic and kinetic data, as well as appropriate software for the simulation of phase transformations at a moving interface of 2 different matrixes, the accurate modeling of compound layer growth kinetics in gaseous nitrocarburizing of iron has yet to be achieved **[5]**.

During a study in two Universities of China, J-Q Sun et al examined gaseous nitriding of cast iron at lower temperature. The nitriding process was applied to a specifically prepared catalytic surface. Surface catalysis is a process used commonly in the industry in order to generate a more efficient surface reaction since it helps the reluctant molecules activate faster and at lower temperatures. The compositions of the cast iron samples that were used are shown in ***Table 2. 1***.

Table 2. 1 : Composition of alloy cast ion.

Element	***C***	***Si***	***Mn***	***Cu***	***Cr***	***B***	***P***	***S***
Concentration (%)	*2.8–3.2*	*1.6–2.0*	*0.7–1.0*	*0.8–1.2*	*0.25–0.4*	*0.03–0.05*	*0.15–0.25*	*<0.12*

The samples were prepared for surface catalysis and then nitride at different temperatures (360 ◦C, 400 ◦C, 450 ◦C, 480 ◦C for 10 h, and 500 ◦C for 4 h, respectively). The experimental results showed that ammonia decomposition on the surface has a higher rate due to the catalytic activity and increases significantly in relation to the temperature. At 400◦C the rate was 5.0% and reached as high as 15.2% at 500◦C. In comparison to untreated samples, the iron specimens that underwent pretreatment exhibited decomposition rate about 5 times higher, which can be shown in ***Figure 2.1. 4***. The obvious result of this study was that the presence of catalysts on the nitriding surface enhances ammonia decomposition, and the produced nitrogen is efficiently absorbed even at lower temperatures **[6].**

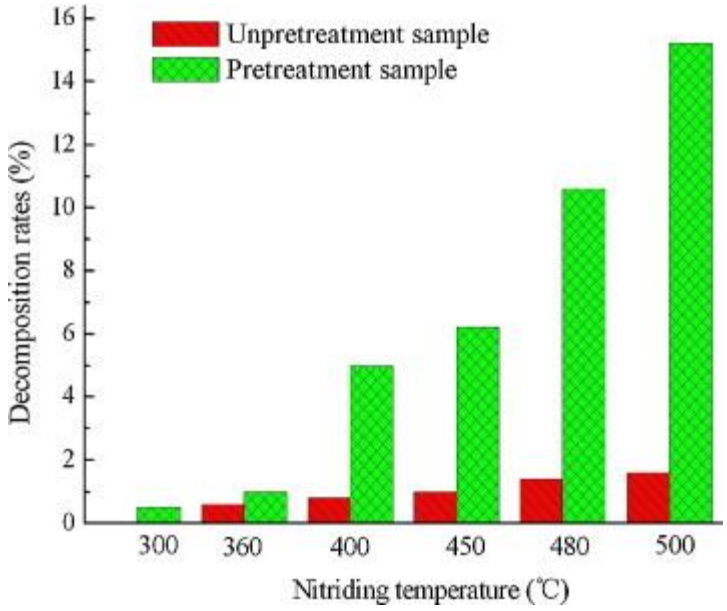

Figure 2.1. 4: Comparison of NH_3 decomposition rates for untreated and pretreated cast iron samples **[6]**.

2.2 Nitriding Mechanism- Diffusion Reaction

Gas nitriding is a heat treatment process that occurs in an atmosphere composed of a mixture of ammonia (NH_3) and hydrogen (H_2). It can take place on iron or steel surfaces with the goal to increase their durability and hardness, as mentioned above. The general chemical reaction that occurs {1} is most likely the result of 2 partial reactions {2} and {3}.

- $NH_3 \leftrightarrow [N] + (3/2)\, H_2$ {1}
- $(1/2)\, N_2 \leftrightarrow [N]$ {2}
- $NH_3 \leftrightarrow (1/2)\, N_2 + (3/2)\, H_2$ {3}

[N] represents the nitrogen atoms dissolved into the octahedral positions of the ferrite or the Fe-nitrides. Reaction {3} represents the decomposition of NH_3 inside the gas mixture provided for the process, while reaction {2} is related to the absorption of nitrogen into the solid ferritic surface during the diffusion. The activity of an element exhibits its tendency to react with other elements or materials and greatly affects the element's diffusion in solid materials. Provided that local equilibrium occurs between the gas phase and the solid solution of N on the ferritic surface, the activity of nitrogen can be calculated by the following equation {4}:

$$\alpha_N = K^{\{1\}} \frac{p_{NH3}}{p_{H2}^{(\frac{3}{2})}} p_0^{2(\frac{1}{2})}$$

In the N activity equation, $K^{\{1\}}$ is the equilibrium constant of reaction {1}, p (NH_3, H_2) are the partial pressures of NH_3 and H_2 gas that are assumed to be ideal and p_0 is the reference pressure chosen at 1atm. Assuming equilibrium, the activity of N that is dissolved can be given by the equation {5}. This parameter is called nitriding potential [r_N] **[5]**.

$$r_N = \frac{p_{NH3}}{p_{H2}^{(\frac{3}{2})}} \quad \{5\}$$

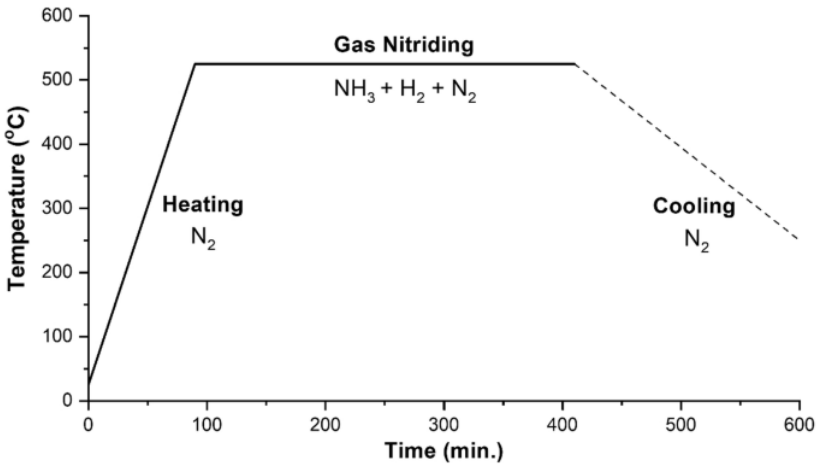

Figure 2.2. 1: The 3 stages of Nitriding Process

In *Figure 2.2. 1*, the 3 stages of the nitriding process are depicted in relation to time. The first step is the material's heating in gaseous nitrogen atmosphere, afterwards the nitriding treatment takes place at about 500-550◦C in ammonia environment. The final step is the cool down process inside a furnace. It is important to note that the total reaction is relatively slow, and the treated specimen could need to be retained inside the furnace for lengthy amounts of time.
Therefore, the nitriding mechanism can be described by the following phases:

1. Ammonia transportation into the iron or steel surface through molecular diffusion.
2. The molecules get absorbed into the interstitial sites of the ferritic lattice and dissociate into atomic nitrogen and hydrogen.
3. Nitrogen diffusion into the outer surface and formation of iron nitrides (Fe_xN), γ' and ε.
4. Hydrogen, in the form of H_2 molecules, reacts with oxygen to generate water vapor, which is then released into the furnace atmosphere.
5. Formation of the Compound Layer on the outer surface and the Diffusion Zone deeper into the material.

In order to achieve a successful nitriding treatment, it is very important for the basic parameters that affect the nitrogen diffusion process to be under control. Those basic influences are the furnace temperature, the duration of treatment, the flow rate of the gas mixture inside the furnace along with the furnace maintenance. Pre-treatments, preheating and texture of the specimen's surface also play an important role in the effectiveness of nitriding and the attainment of the desired final microstructure that leads to a hardened, more durable and resistant iron or steel surface.

2.3 Material under Examination

The material used for this thesis is a novel ductile cast iron with composition Fe- 3.4%C- 4%Si- 1%Nb and (0-4) wt% Al. This cast iron was chosen to be studied in the search for new improved materials capable of enduring thermal and mechanical stresses as well as being resistant to oxidation environments. Ferritic alloys exhibit high thermal conductivity and low thermal expansion [7], are lower-cost than austenitic steels and show great high-temperature strength. In order to satisfy industry demand, a study by Çelik, Haidemenopoulos et al was conducted with the goal to achieve the appropriate ferritic alloy design which could replace the use of commercial ferritic ductile cast iron in cases of demanding conditions [8].The chemical compositions of the cast alloys strongly influence the transformation temperatures and thermal and mechanical properties of the material. For the enhancement of these properties, a higher *A1* temperature is desired. It is called the eutectoid temperature, it represents the lowest critical temperature in the iron-carbon phase diagram, and it corresponds to the lowest temperature for stable austenite (γ). In designing the ductile cast iron alloys, a hypereutectic composition of carbon (C) and silicon (Si) should be used to obtain a hypereutectic C equivalent (≥4.7) for casting and solidification. This is utilized to accomplish high graphite nodularity, high nodule count, as well as homogenous graphite distribution in the cast iron alloy [9], Presence of Si achieves increase of A1 temperature, as well as the addition of Al, Ti, Nb and W [10], [11]. Ti and Nb addition enhance mechanical properties through the formation of carbides that remain stable in higher temperatures [12], [13]. It is believed that these 2 alloying elements cause a transformation of spheroidal graphite nodules spiral shaped [14], [15], [16]. On one hand this transformation improves thermal conductivity [17] while on the other, the iron's mechanical properties are somewhat negatively affected [18], [19].

- Mechanicals properties are also enhanced by the addition of Mo, W and Cr of composition of up to 1wt%.
- Other than A1 temperature increase, aluminum (Al) presence also offers the creation of an oxide layer at elevated temperature that results in oxidative resistant ferritic cast iron [20].

CHAPTER 3: Thermodynamic Calculations

3. THERMOCALC - Computational Tool

THERMOCALC is widely considered to be the best tool for calculations of thermodynamic data and phase diagrams, especially for multi-component alloys. A large variety of databases is available for use, each containing different groups of material, such as Steel/Fe-alloys, Ni-alloys, Cu-alloys and Al-alloys. This powerful software has the capacity to compute stable, as well as metastable equilibrium of heterogenous phases, phase diagrams, the percentage of phases in the system, phase compositions, thermodynamic properties and phase transformation temperatures. It provides a great variety of information while studying a material's microstructure, being able to predict its final form in relation to specific variables and ultimately compare it to experimental results if needed. The science of materials greatly benefits from the use of this user-friendly software.

3.1 Phase Diagrams, Phase Fractions, Composition of α-phase

As the first step in the thermodynamical approach of the nitriding process, the phase diagrams of the specific cast iron A80 {Fe- 3.4C- 4.0Si- 1Nb- 10N- (0-4%wt) Al} were calculated, in order to, determine the material's initial microstructure at the nitriding temperature (783K) and in relation to Nitrogen content. The thermodynamic database TCFE11: Steels/Fe Alloys of THERMOCALC was used for the calculations, all phases were suspended and then only the expected phases were restored. Those phases were the following:

1. α -ferritic phase (BCC)
2. γ- austenitic phase (FCC)
3. Liquid phase (L)
4. Cementite phase
5. Graphite phase (G)
6. FCC#2 or NbN phase
7. ε-nitride / HCP phase
8. γ'- nitride / Fe_4N phase
9. AlN phase
10. Si_3N_4 phase
11. κ-carbide (KAPPA) / Al-rich carbide

The vertical axis (y) of the diagram indicates the temperature in degrees Celsius, while the horizontal axis (x) presents the N composition of the material from 0 to 13 wt.% (weight percent). The calculations were performed under constant pressure of 1atm, as well as, constant composition of all other alloying elements, gradually increasing the composition of Al by 1.0wt% in every calculation. ***Figure 3.1. 1*** shows the phase diagram of the cast iron without any aluminum content (0%Al) while ***Figure 3.1. 2, Figure 3.1. 3, Figure 3.1. 4, and Figure 3.1. 5*** depict the corresponding isopleths of aluminum content 1wt%, 2wt%, 3wt% and 4wt% accordingly.

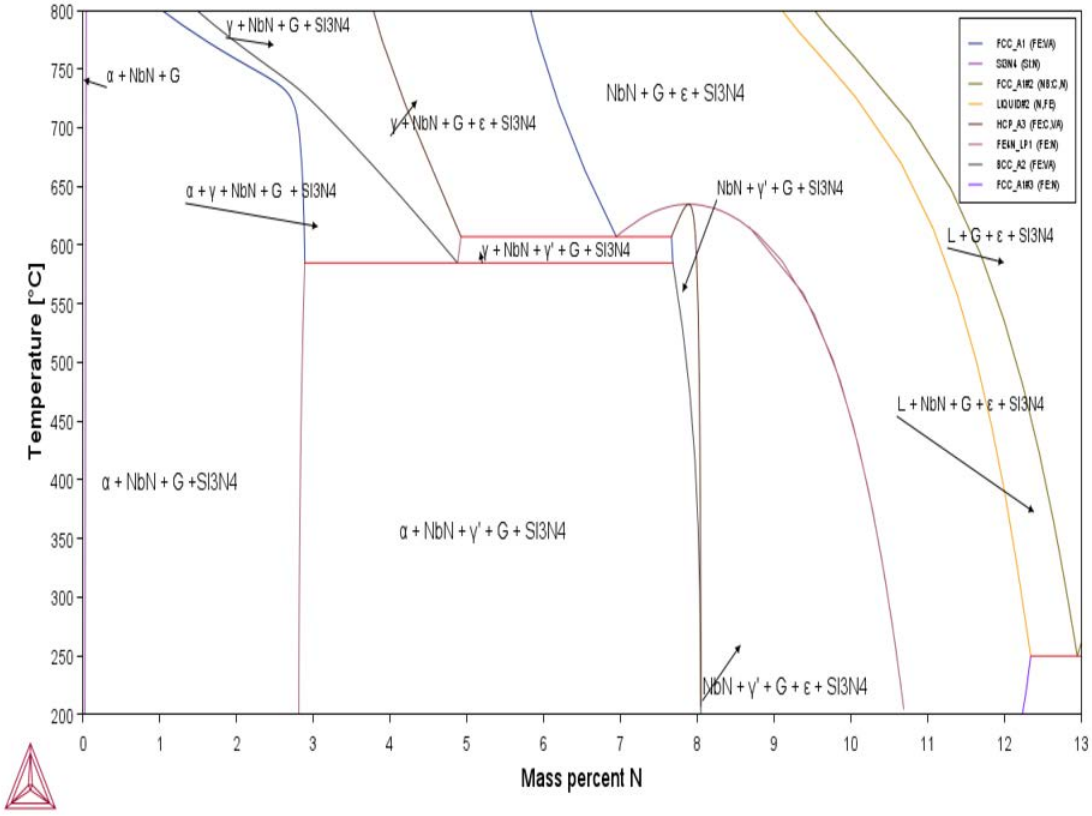

Figure 3.1. 1: Phase Diagram of cast iron A80 Fe- 3.4C- 4.0Si- 1.0Nb- 10.0N- (0wt%) Al

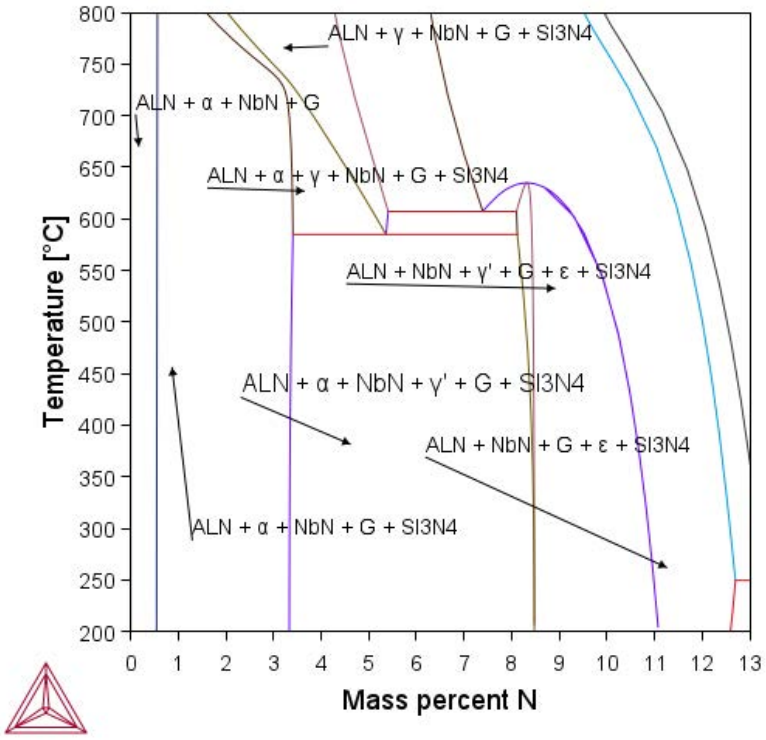

Figure 3.1. 2: Phase Diagram Fe-3.4C-4.0Si-1.0Nb-10N- (1.0wt%) Al

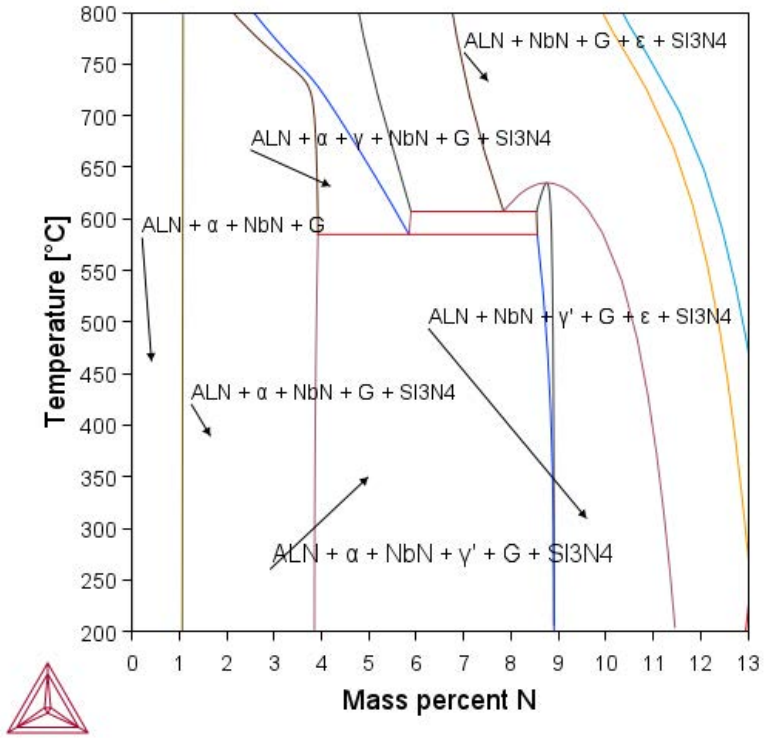

Figure 3.1. 3: Phase Diagram Fe-3.4C-4.0Si-1.0Nb-10N- (2.0wt%) Al

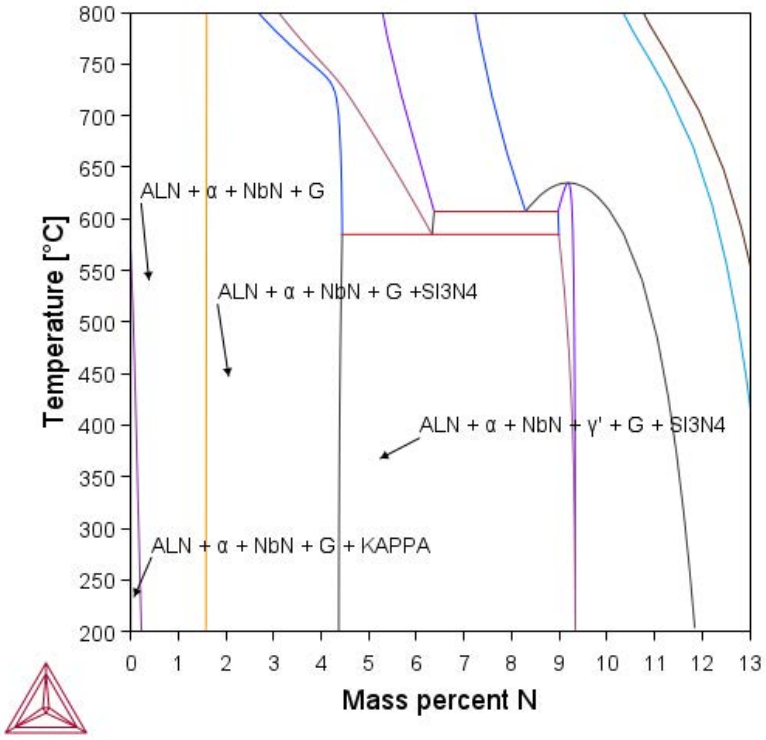

Figure 3.1. 4: Phase Diagram Fe-3.4C-4.0Si-1.0Nb-10N- (3wt%) Al

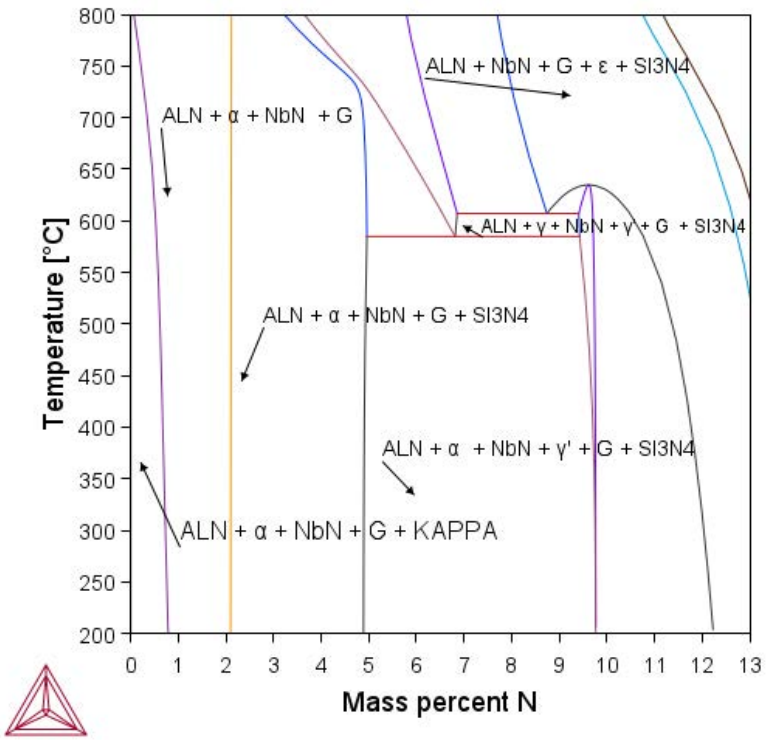

Figure 3.1. 5: Phase Diagram Fe-3.4C-4.0Si-1.0Nb-10N- (4wt%) Al

It can be noted that with the addition of aluminum, κ-carbide becomes gradually evident, which is a logical outcome considering it is a phase rich in Al. It is also shown that at the specified nitriding temperature of 510◦C (783Kelvin) the microstructure follows the same journey of formed phases along the x axis (N composition) for all Al compositions calculated.

These phase diagrams offer us a way to correspond the distance (x) of the cast iron surface to the weight percentage of N (0-13wt%). This will become useful during the nitriding process, in order to differentiate the diffusion surface in 2 stages. The diffusion zone, consisting of ferrite with dispersed phases of graphite, γ'-nitride (Fe_4N), AlN, NbN and Si_3N_4, as well as the compound layer which consists of three distinct areas. A γ'area, a γ'+ε area and an ε phases area. This happens due to the low solubility of nitrogen into ferrite which creates ε and γ' nitrides in sediment form. The diffusion zone and compound layer is be shown in ***Figure 3.1. 6***.

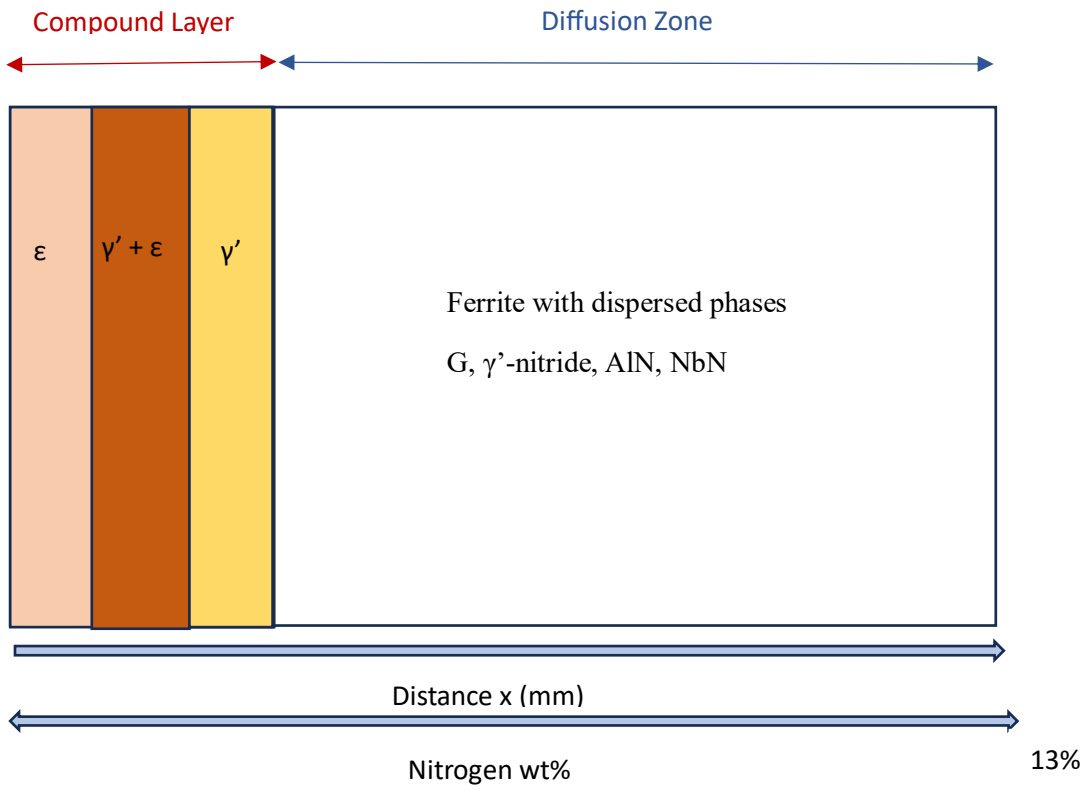

Figure 3.1. 6: Representation of the diffusion zone and compound layer formed on cast iron surface during nitriding process due to ε and γ' nitride in correspondence to wt% of nitrogen

Afterwards, the phase fractions of the system were calculated, in order to determine the percentages of each phase under a specific set of conditions. The temperature was set at 510◦C and the pressure at 1 atm. The calculations were made for the same cast iron compositions, the aluminum content increasing from 0 to 4 wt%. The effect of aluminum addition in the cast iron material can be shown in ***Figure 3.1. 7***, ***Figure 3.1. 8***, ***Figure 3.1. 9***, ***Figure 3.1. 10*** and ***Figure 3.1. 11***. The γ' and ε nitrides start formation at higher nitrogen contents with the increase of Al and the Si_3N_4 phase is also pushed to higher nitrogen levels. The amount of AlN phase is obviously increased by the added Al and the α-ferritic phase is expanded from about 7.9wt% N (0%AL) to about 9.6wt% N (4%Al). The Al-rich κ-carbide becomes visible with the final addition of 4wt% Al in the lower N contents. It is logical to assume that in case of further aluminum addition κ-carbide would follow the same behavior as the γ' (Fe_4N) and ε (HCP) carbides, being pushed to higher nitrogen contents. The amount of Graphite phase seems to remain stable with the Al additions and the amount of NbN phase seems constantly low, almost non-existent in all the following figures.

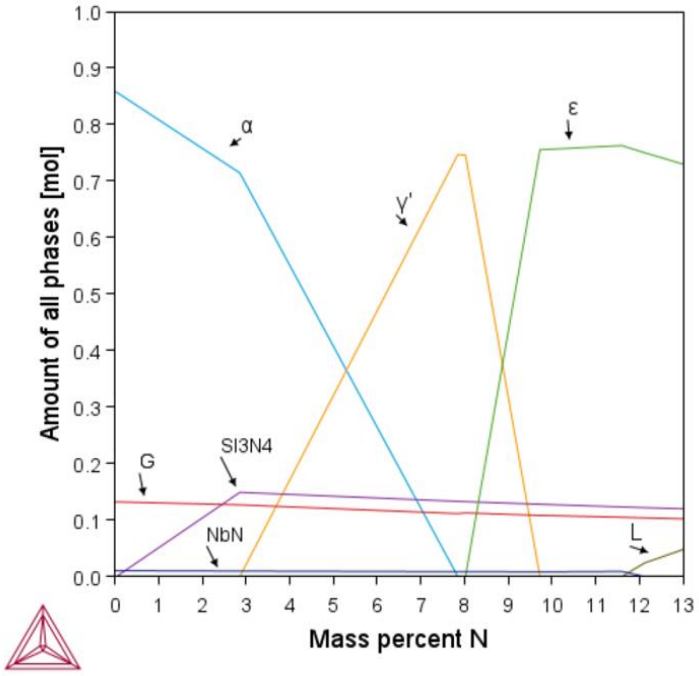

Figure 3.1. 7: Phase Fractions of Fe-3.4C-4.0Si-1.0Nb-10N- (0wt%) Al

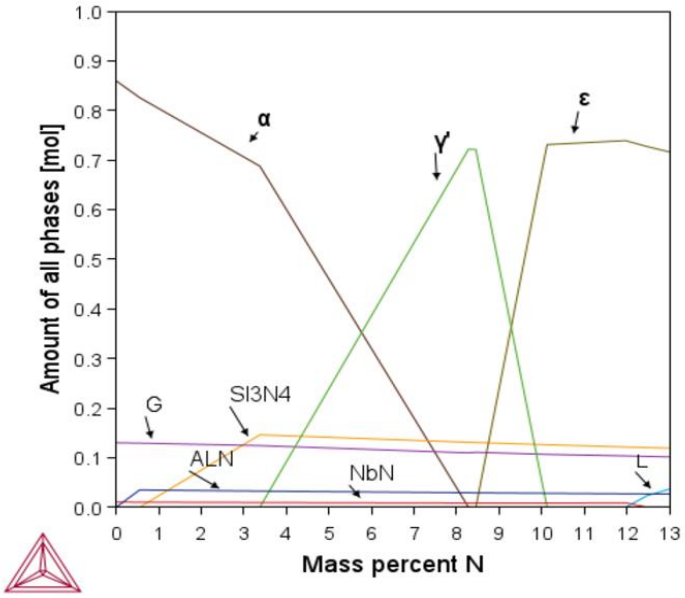

Figure 3.1. 8: Phase Fractions of Fe-3.4C-4.0Si-1.0Nb-10N- (1wt%) Al *[right]*

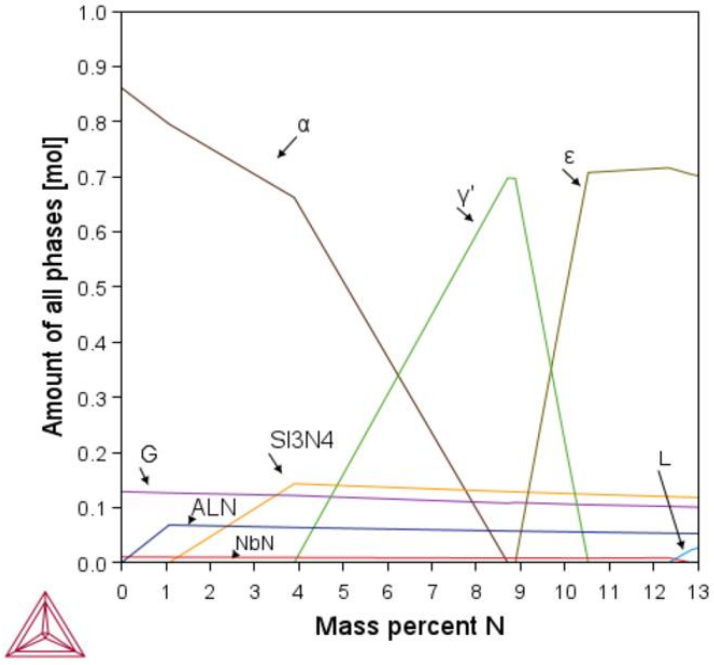

Figure 3.1. 9: Phase Fractions of Fe-3.4C-4.0Si-1.0Nb-10N- (2wt%) Al *[left]*

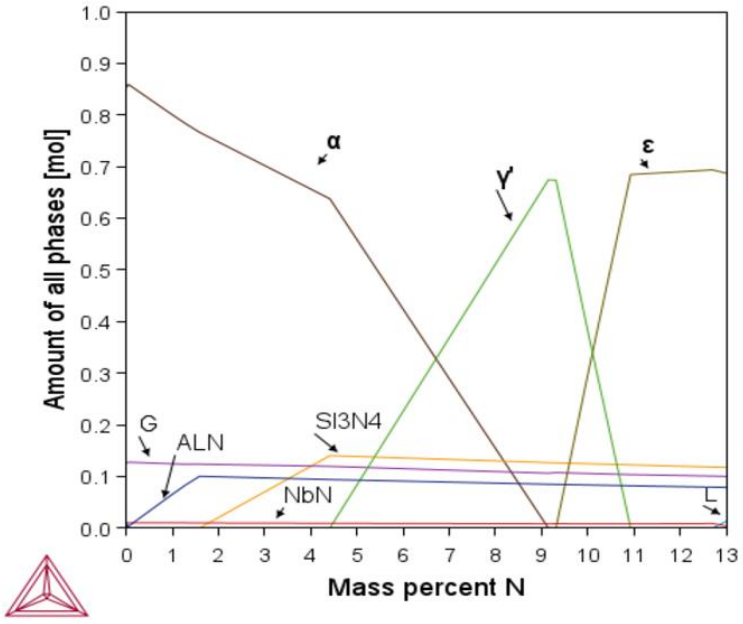

Figure 3.1. 10: Phase Fractions of Fe-3.4C-4.0Si-1.0Nb-10N-(3wt%) Al *[right]*

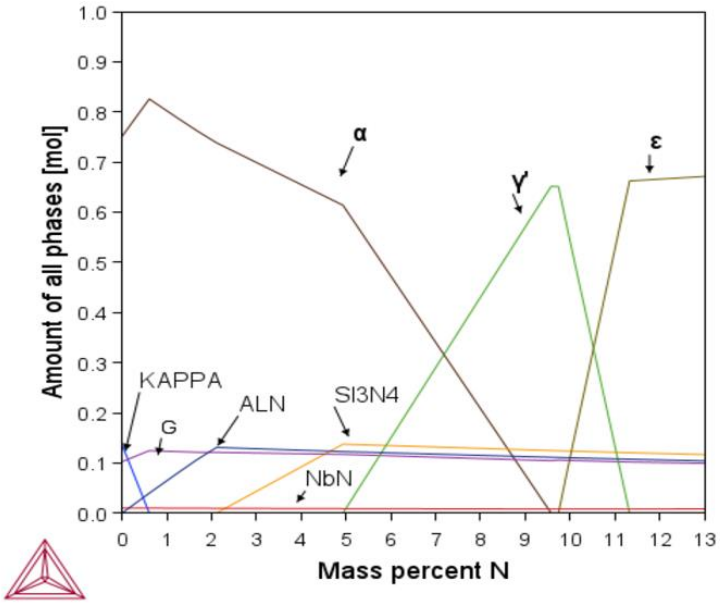

Figure 3.1. 11: Phase Fractions of Fe-3.4C-4.0Si-1.0Nb-10N- (4wt%) Al at 510◦C

The next step of this project's process was for the graphs containing the composition of all alloying elements in BCC α-phase to be calculated. These graphs are useful, in order to determine the amount of all the alloying elements that is contained in the ferritic phase, which will be used as the base in which the rest of the phases will be dispersed, as shown in ***Figure 3.1. 6***.

The results of those calculations can be shown in ***Figure 3.1. 12***, ***Figure 3.1. 13, Figure 3.1. 14***, ***Figure 3.1. 15*** and ***Figure 3.1. 16*** for every Al composition 0-4wt%. The Nb mass percentage was barely visible during the calculation process which means that the amount of NbN phase is BCC is very minimum. For each case the graph has been zoomed in, in order to determine the amount of N, Si, C and Al components in the ferritic phase at the same 510◦C temperature which will be used during the nitriding process in later stages of this project.

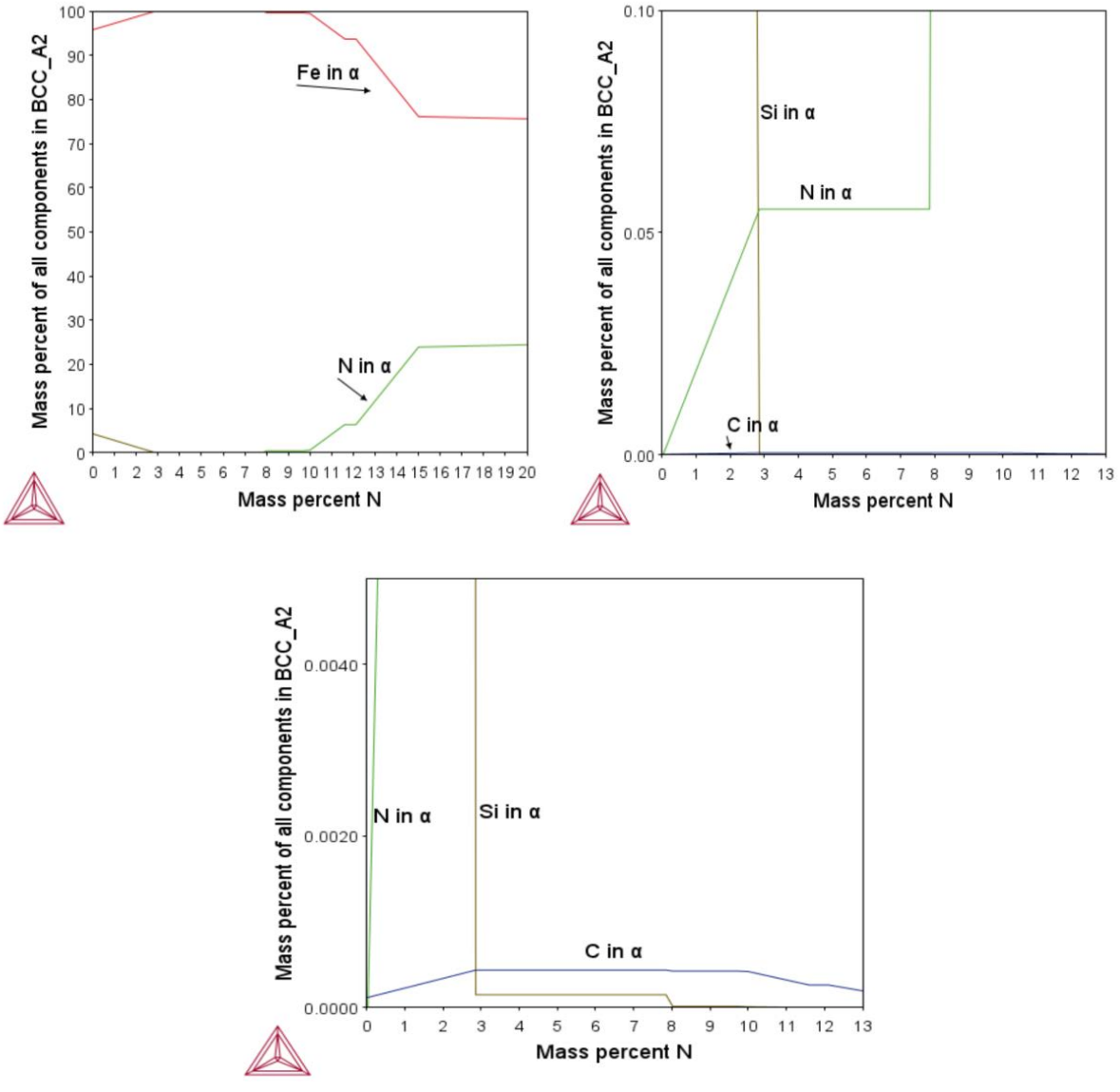

Figure 3.1. 12: Composition of alloying elements (Fe, N, Si, C, Nb, Al) for 0wt%Al at 510◦C

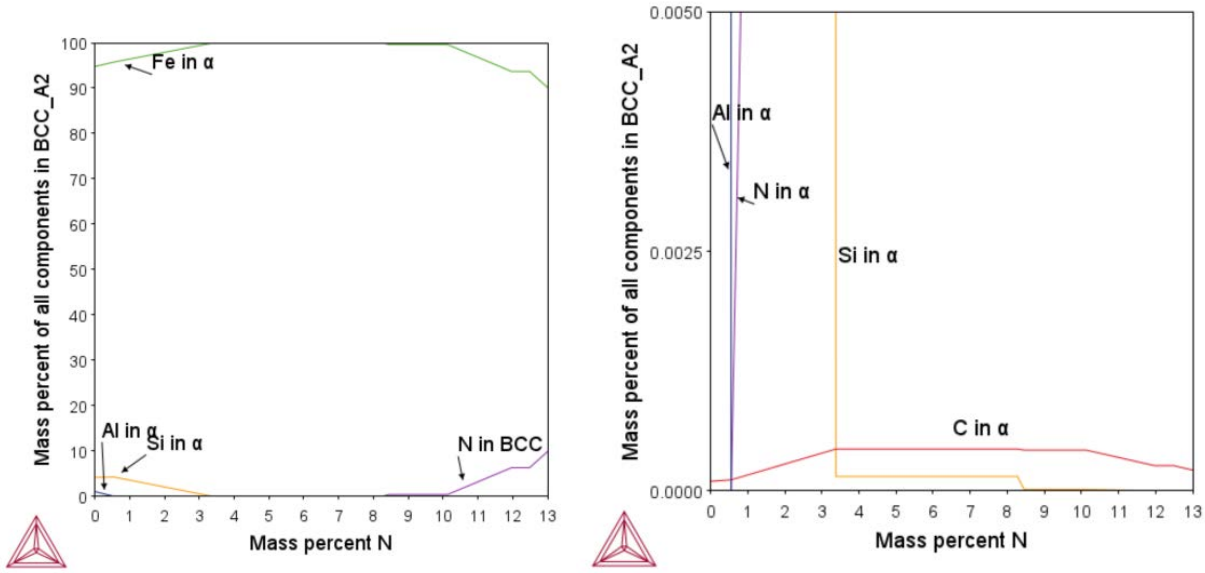

Figure 3.1. 13: Composition of alloying elements (Fe, N, Si, C, Nb, Al) for 1wt%Al at 510◦C

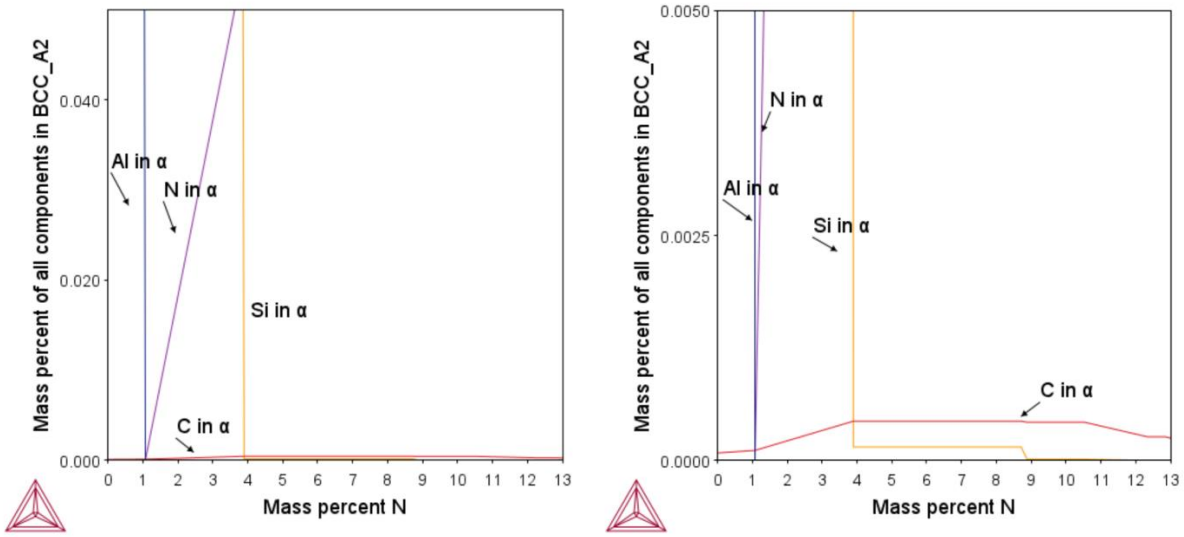

Figure 3.1. 14: Composition of alloying elements (Fe, N, Si, C, Nb, Al) for 2wt%Al at 510◦C

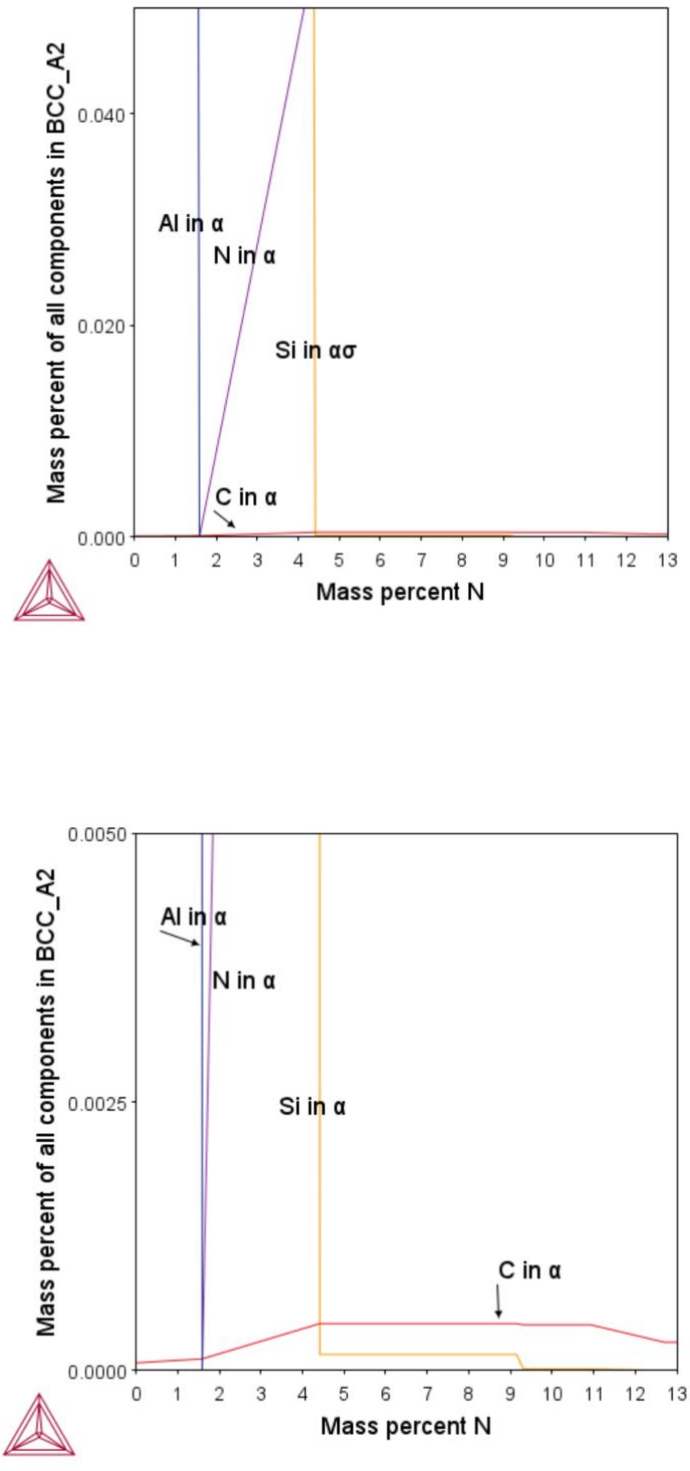

Figure 3.1. 15: Composition of alloying elements (Fe, N, Si, C, Nb, Al) for 3wt%Al at 510◦C.

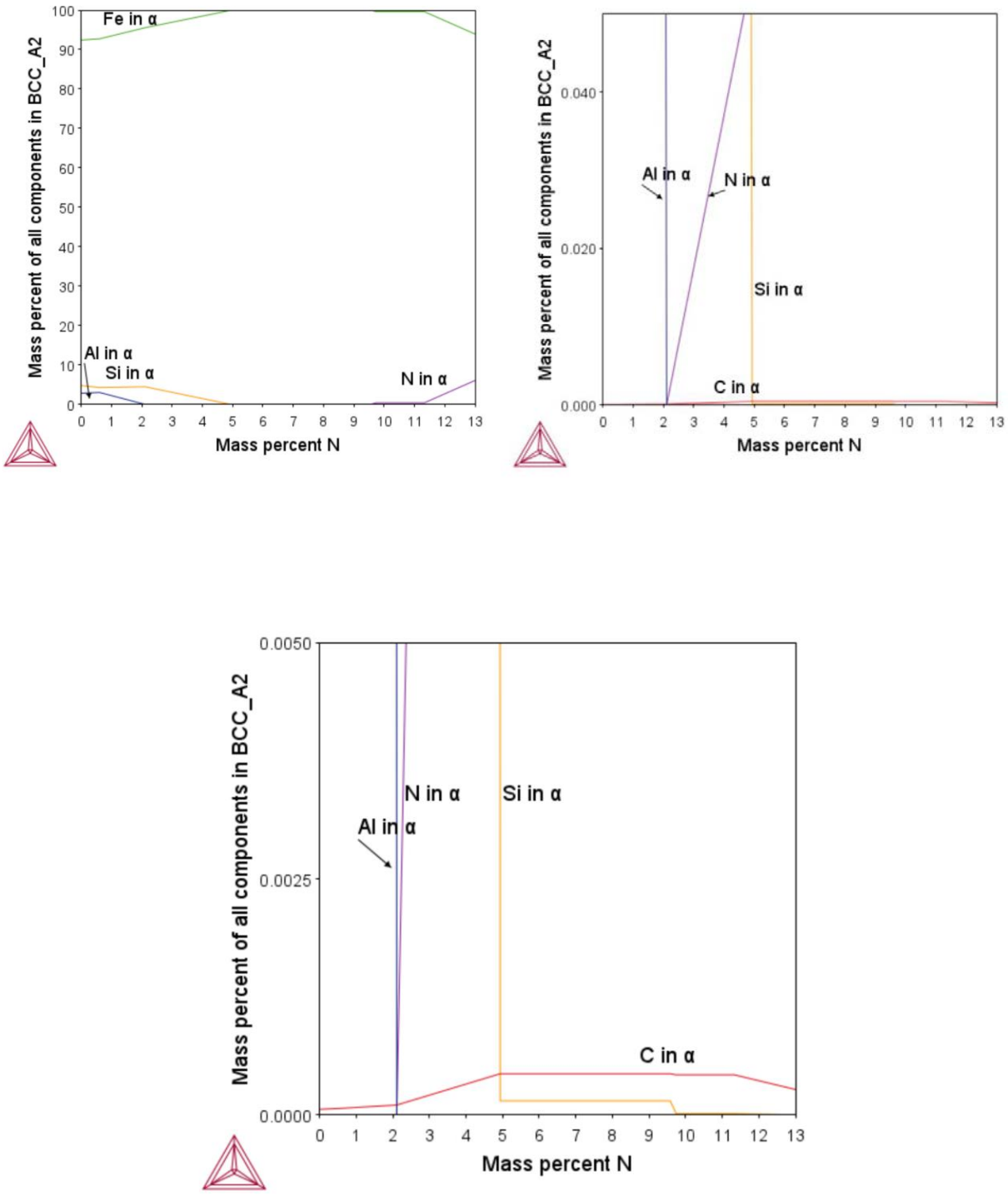

Figure 3.1. 16: Composition of alloying elements (Fe, N, Si, C, Nb, Al) for 4wt%Al at 510◦C

3.2 Suspension of Si_3N_4 & Thermodynamic Calculations

The experimental results of the cast iron's nitriding process revealed that the phase Si_3N_4, ultimately was not formed. That is why it was imperative to repeat the previous thermodynamic calculations, suspending the Si_3N_4 phase. A difference is visible in the phase diagrams shown in ***Figure 3.2. 1*** and ***Figure 3.2. 2*** for Al composition (0-3) wt%, not including the Si_3N_4-phase.

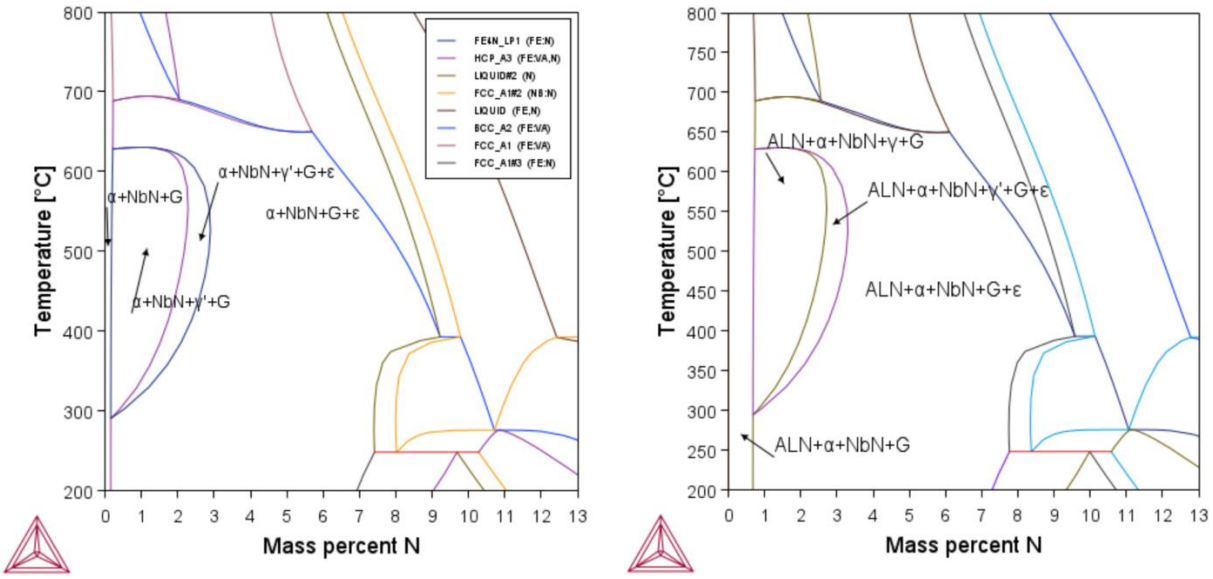

Figure 3.2. 1: Phase diagrams of cast iron Fe-3.4%C-4.0%Si-1.0%Nb-10%N, suspended Si_3N_4 phase, for 0wt%Al *[left]* and 1wt%Al *[right]*

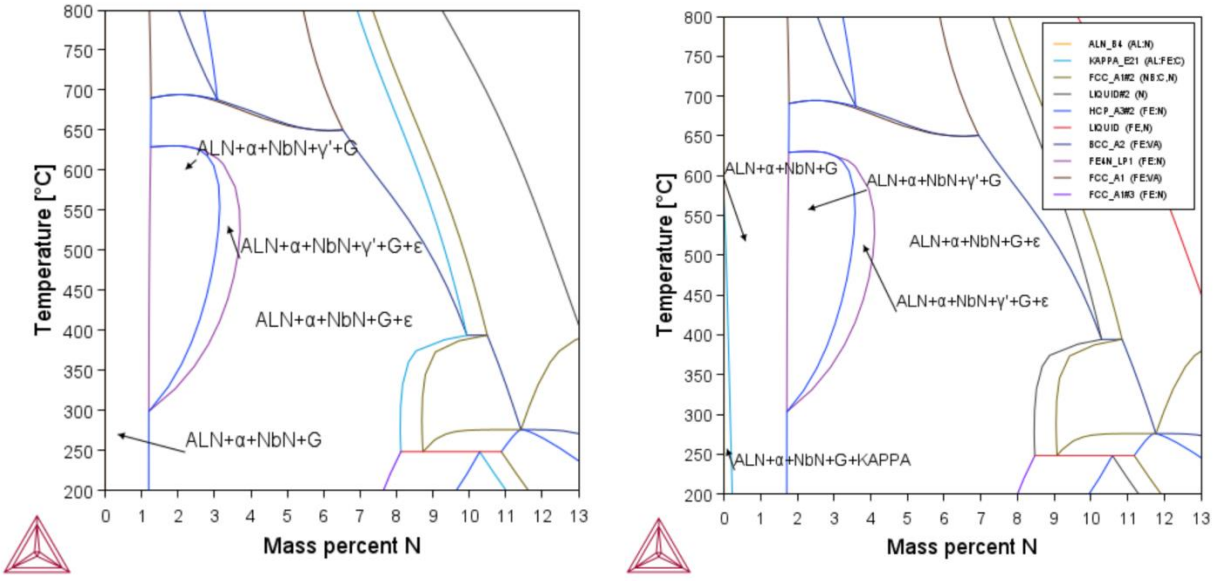

Figure 3.2. 2: Phase diagrams of cast iron Fe-3.4%C-4.0%Si-1.0%Nb-10%N, suspended Si_3N_4 phase, for 2wt%Al *[left]* and 3wt%Al *[right]*

The comparison between the phase diagrams of the material with 4wt% Al content including and suspending phase Si_3N_4 are shown in ***Figure 3.2. 3***.

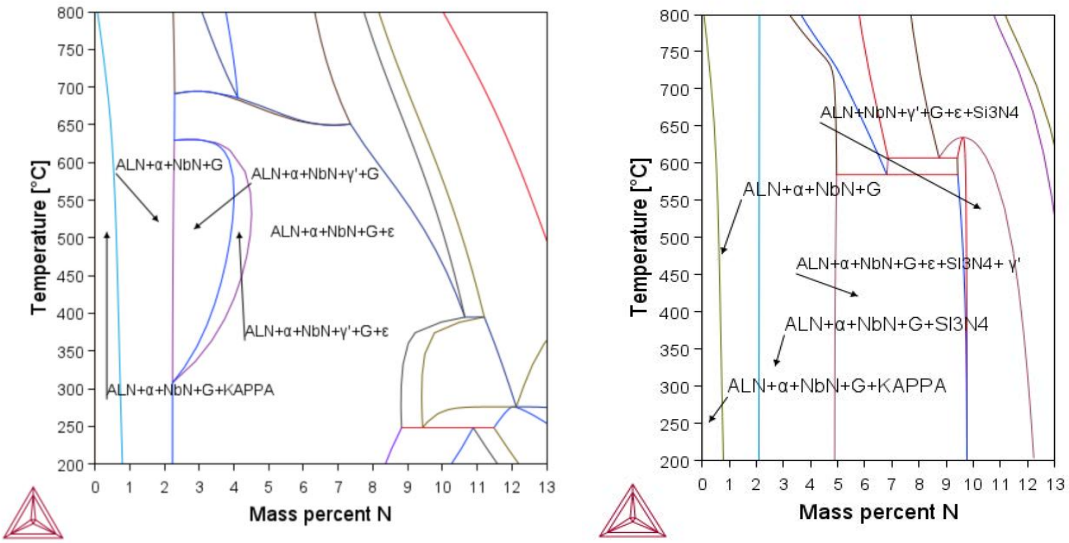

Figure 3.2. 3: Phase diagrams of cast iron Fe-3.4%C-4.0%Si-1.0%Nb-10%N with 4%Al without phase Si_3N_4 *[left]* and including phase Si_3N_4 *[right]*

Apart from the lack of the suspended phase Si_3N_4, looking at the temperature of 510◦C, the biggest difference that can be determined is that the formation of γ' (Fe_3N_4) carbides takes place in lower nitrogen contents in comparison. The same implies for the ε (HCP) phase.

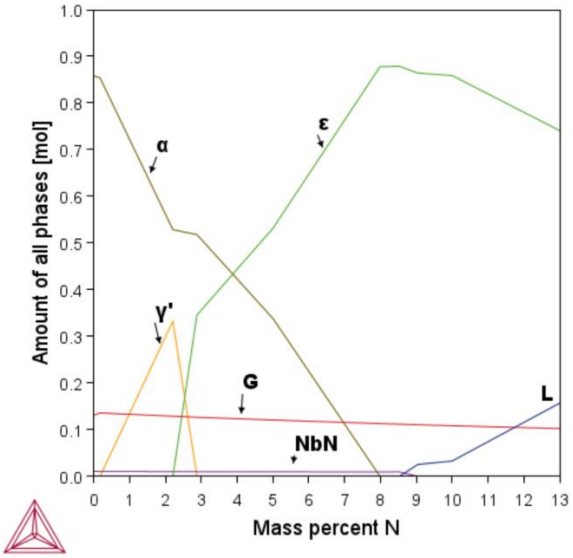

Figure 3.2. 4: Phase Fractions of Fe-3.4C-4.0Si-1.0Nb-10N- (0wt%) Al -*510◦C*-Si_3N_4 suspended.

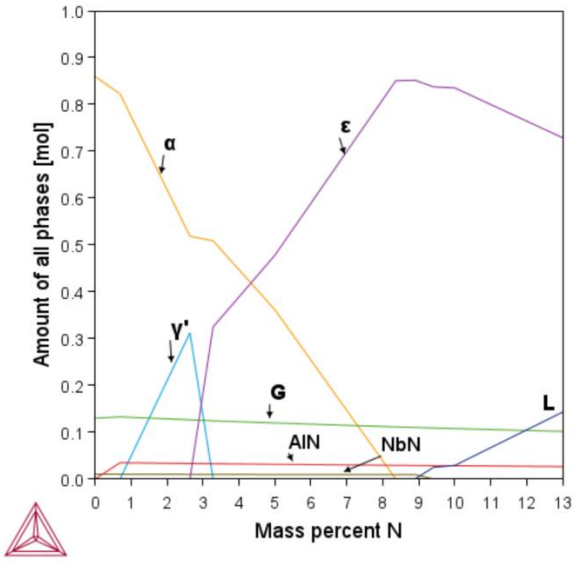

Figure 3.2. 5: Phase Fractions of Fe-3.4C-4.0Si-1.0Nb-10N-(1wt%) Al-*510◦C*-Si_3N_4 suspended.

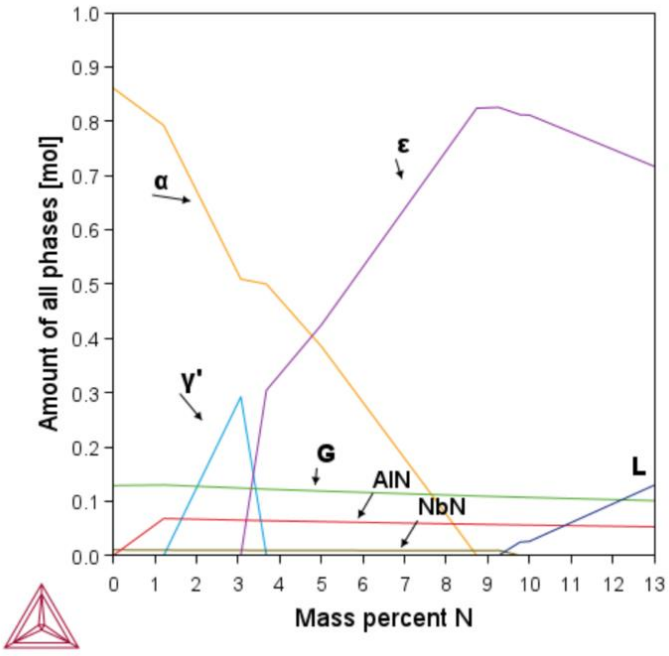

Figure 3.2. 6: Phase Fractions of Fe-3.4C-4.0Si-1.0Nb-10N- (2wt%) Al *[left]- 510◦C*-Si_3N_4 suspended.

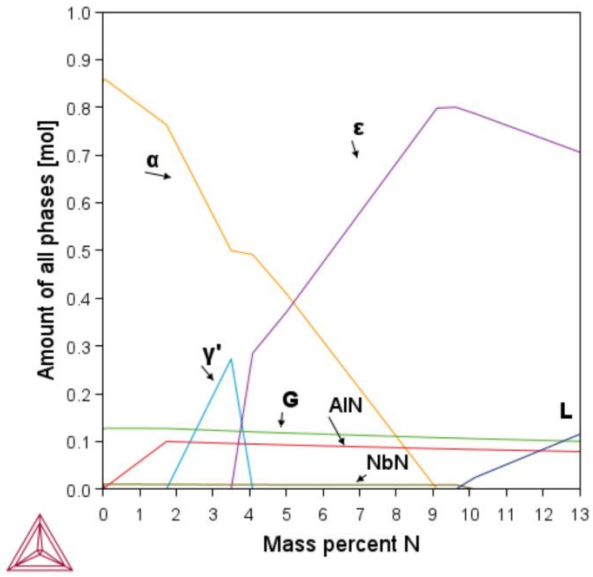

Figure 3.2. 7: Phase Fractions of Fe-3.4C-4.0Si-1.0Nb-10N-(3wt%) Al *[right]-510◦C*-Si_3N_4 suspended.

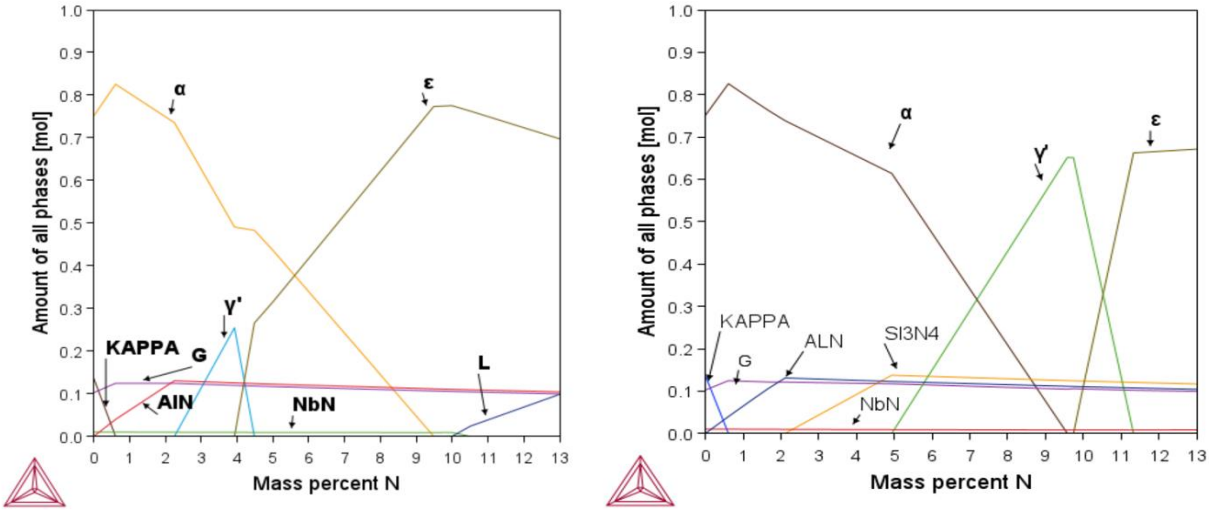

Figure 3.2. 8: Phase Fractions of Fe-3.4C-4.0Si-1.0Nb-10N- (4wt%) Al-*510◦C*-Si_3N_4 suspended *[left] &* including Si_3N_4 phase *[right]*.

Comparing the phase fraction graphs that were calculated after the suspension of phase Si_3N_4 *(**Figure 3.2. 4**, **Figure 3.2. 5**, **Figure 3.2. 6**, **Figure 3.2. 7** and **Figure 3.2. 8**)* to those including the phase, it is easy to verify that the γ'-carbides are formed in lower nitrogen contents. It is also evident that the amount of the phase γ' in the system for the specific temperature (510◦C) is significantly less. With the Si_3N_4 phase suspended the percentage of γ' doesn't reach higher than about 34%, decreasing with the addition of Al to 25%, while previously the maximum amount reaches as high as 74%. The nitrogen ranges of γ'-phase for the two cases and different Al compositions are shown in the following ***Table 3. 1***:

wt%Al	**wt%N range for γ' with** Si_3N_4	**wt%N range for γ', no** Si_3N_4
0%	(2.92 – 9.7) wt% N	(0.24 – 2.83) wt% N
1%	(3.44 – 10.1) wt% N	(0.75 – 3.26) wt% N
2%	(3.95 – 10.5) wt% N	(1.27 – 3.66) wt% N
3%	(4.47 – 10.9) wt% N	(1.79 – 4.06) wt% N
4%	(4.9 – 11.3) wt% N	(2.31 – 4.46) wt% N

Table 3. 1: Comparison of wt%N ranges before and after Si_3N_4 suspension for (0-4) wt% Al content.

For the final step of the thermodynamic calculations, it was necessary to create the graphs showing the composition of each of the alloying components (C, Si, N, Nb and Al) in the a-ferritic phase [BCC], the base in which the other phases are dispersed during nitriding. The calculations were also made at nitriding temperature (510◦C), in relation to nitrogen composition along the x-axis (0-13wt%). ***Figure 3.2. 9***, ***Figure 3.2. 10***, ***Figure 3.2. 11***, ***Figure 3.2. 12*** and ***Figure 3.2. 13*** depict those calculations for different Al compositions (0-4wt%).

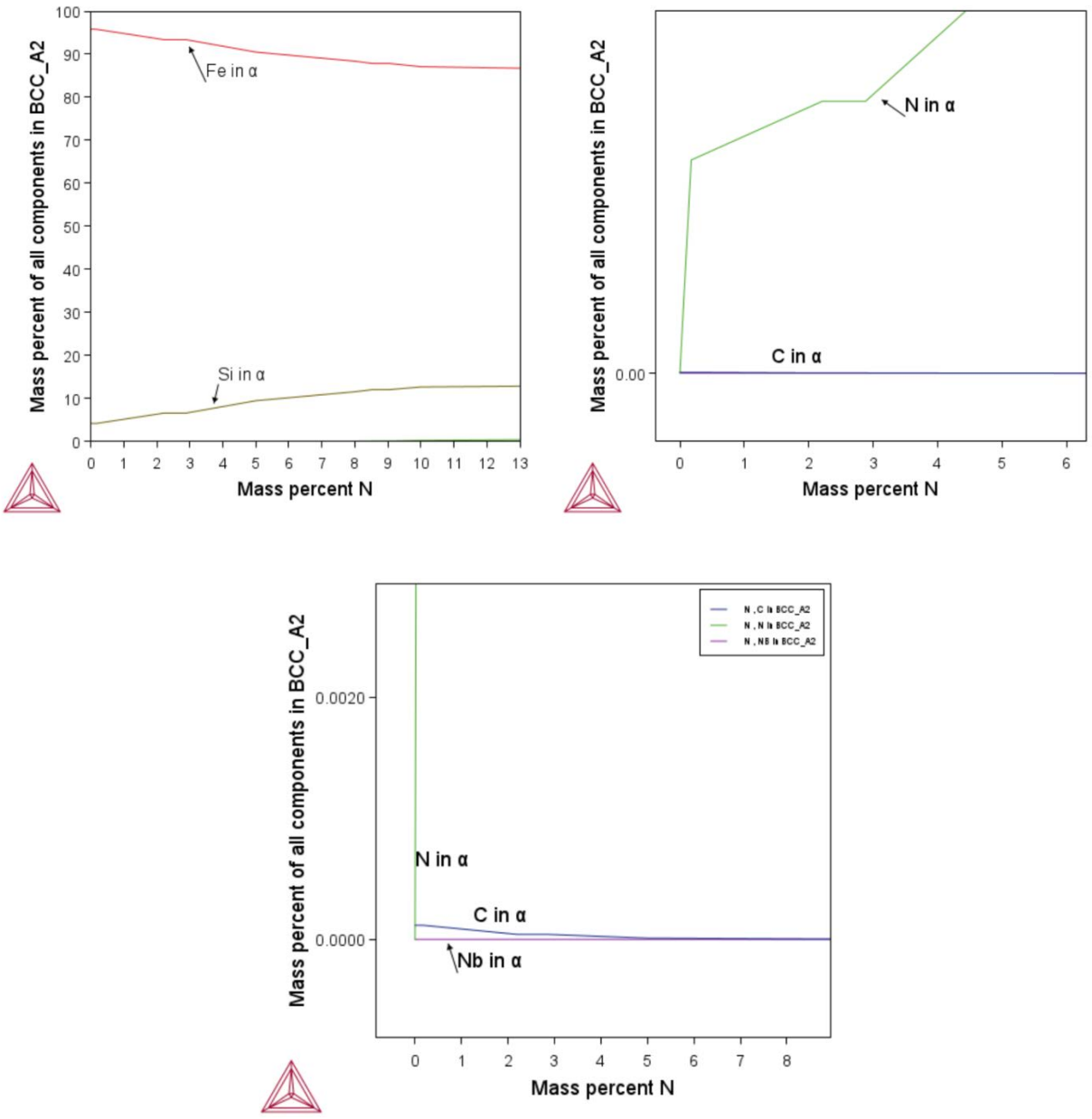

Figure 3.2. 9: Composition of alloying elements in BCC (α) phase- 0%Al- 510◦C

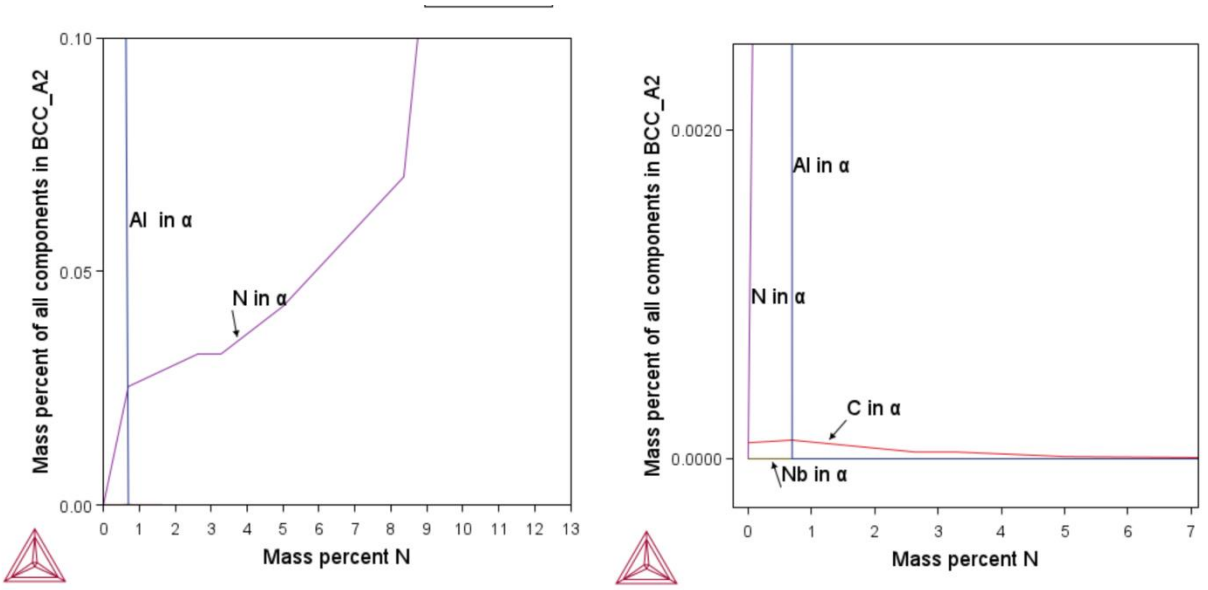

Figure 3.2. 10: Composition of alloying elements in BCC (α) phase- 1%Al- 510◦C

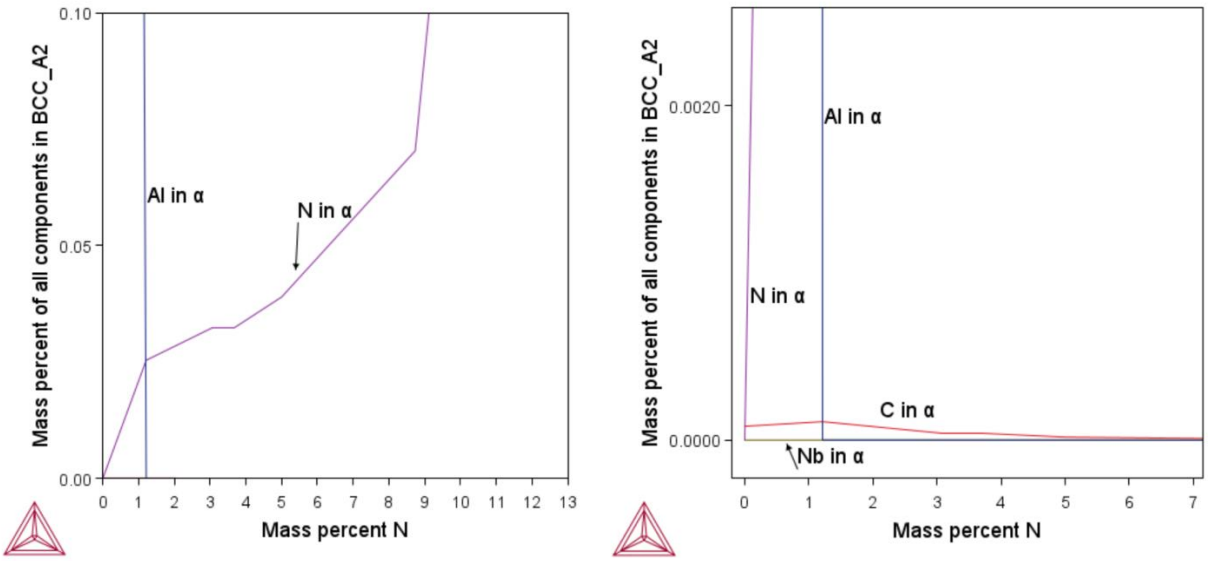

Figure 3.2. 11: Composition of alloying elements in BCC (α) phase- 2%Al- 510◦C

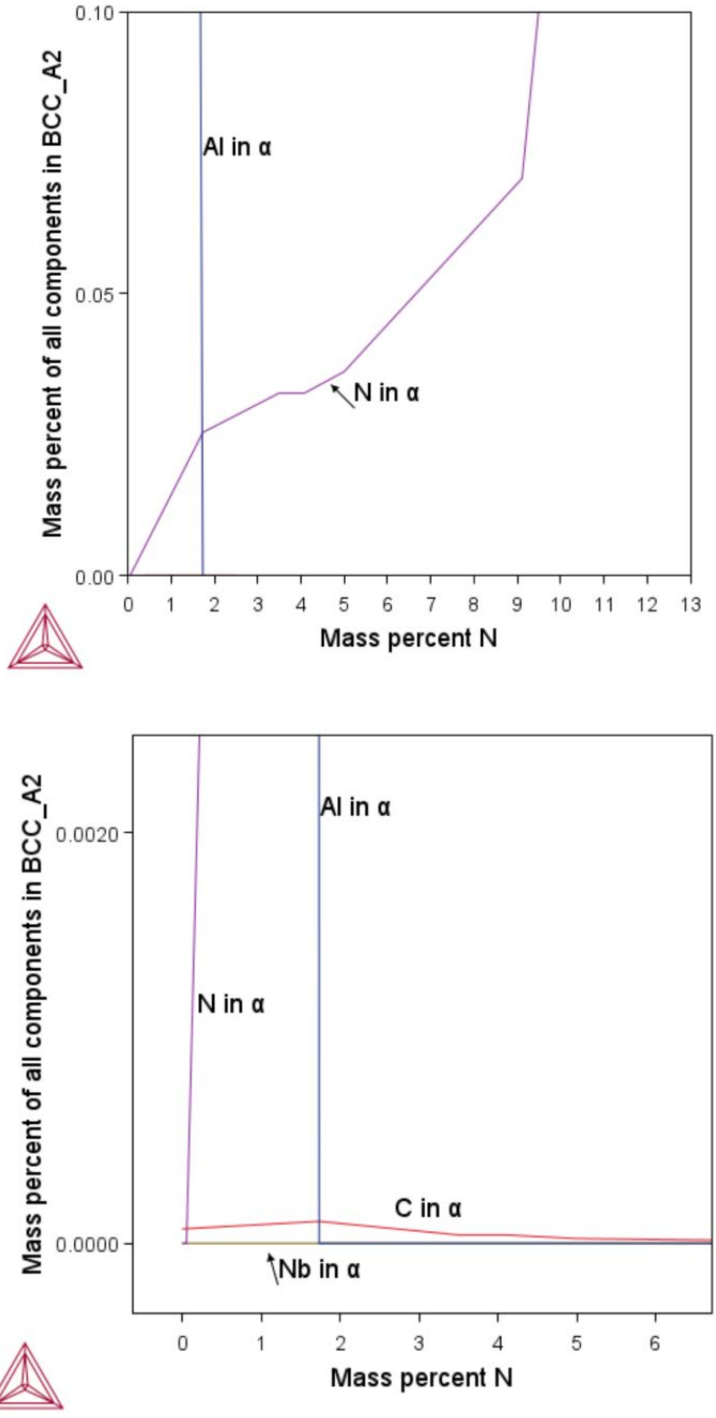

Figure 3.2. 12: Composition of alloying elements in BCC (α) phase- 3%Al- 510◦C

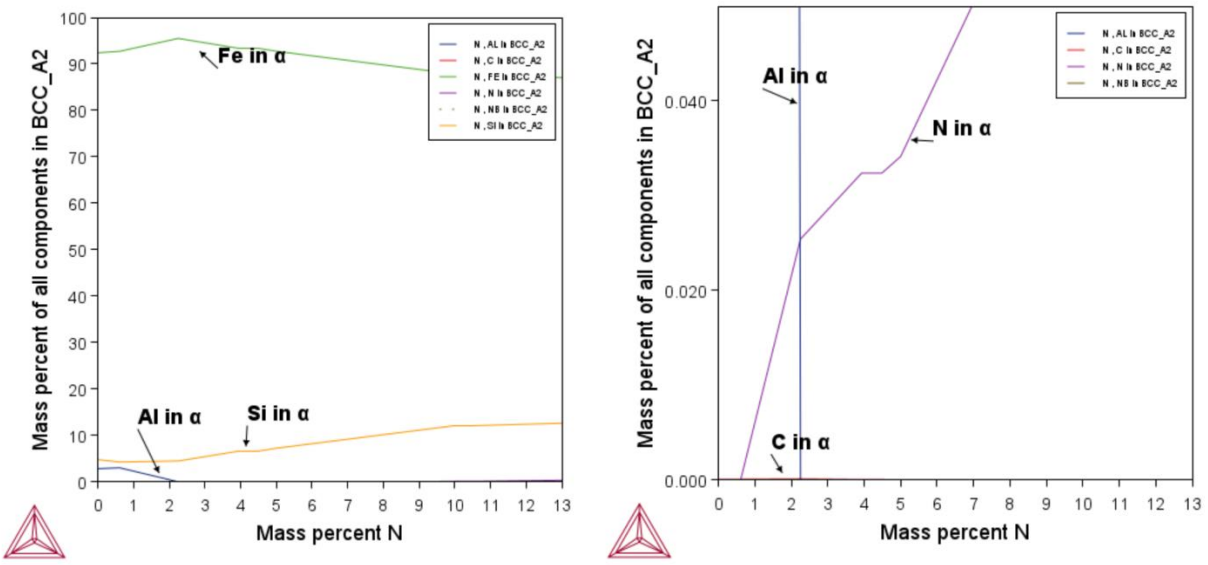

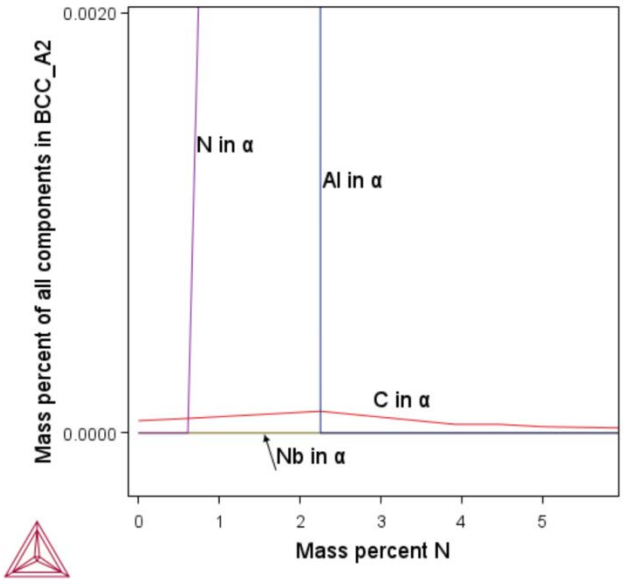

Figure 3.2. 13: Composition of alloying elements in BCC (α) phase- 4%Al- 510◦C

CHAPTER 4: Nitriding- Kinetic Simulations

4.1 DICTRA- Simulation Tool

The acronym DICTRA stands for Diffusion Controlled TRAnsformations in multi-component materials and is a computational tool, part of the Thermo-calc software described above. It is widely applied in metallurgy processes such as heat treatments, welding and alloy design. DICTRA is used for the simulation of phase transformations caused by diffusion (solidification, precipitation, dissolution) in systems consisting of multiple alloying components. It works by combining the diffusion calculations with the thermodynamic data using Thermo-calc databases in equilibrium to model the evolution of each phase during transformations. DICTRA is crucial for industries aiming to enhance material performance by accurately controlling microstructures throughout manufacturing processes.

4.2 Analytic Solution

Nitriding, as a heat-treating process, is characterized by the most important kinetic mechanism, the diffusion of nitrogen atoms inside the ferritic lattice, by jumping from one interstitial position to the next. Fick's 2nd Law of Diffusion is capable of estimating the variation in nitrogen concentration at a specific surface depth in relation to time [4]. In the corresponding equation {4.a} below, c(x,t) represents nitrogen concentration and D(c) is the diffusion coefficient. The diffusion coefficient in reality is dependent to the concentration profile c(x,t), however for this solution it is assumed to be independent. Other condition assumptions concern the vertical to the surface direction of the diffusion, as well as the temperature being a constant variable throughout the process.

$$\frac{\partial c}{\partial t} = \frac{\partial}{\partial x}\left[\, \mathrm{D}(c)\, \frac{\partial c}{\partial x} \right] \qquad \{4a\}$$

In order to solve the nitriding problem, it should be treated as a moving boundary diffusion problem, same as carburization, studying the movement of the interfaces between the dominant ferritic phase and phases γ'and ε that form inside the compound layer during the diffusion. ***Figure 4.2. 1*** presents the phase diagram in correspondence to the depth of the surface.

The x-axis showing the concentration of nitrogen in relation to temperature is turned sideways and is transformed into the y-axis on the right graph, exhibiting the nitrogen concentration in relation to surface depth. The interface between α and γ' phase is visible at distance λα from the surface, while the addition of nitrogen starts the diffusion by abruptly increasing the concentration of nitrogen from the boundary point A ($c_0 = 0$) to point B. Solving Fick's law would lead to the general form of the equation representing the diffusion of each phase (α, γ', ε) {4.b}.

$$C(x,t) = A + B\,erf\left(\frac{x}{2\sqrt{Dt}}\right) \qquad \{4.b\}$$

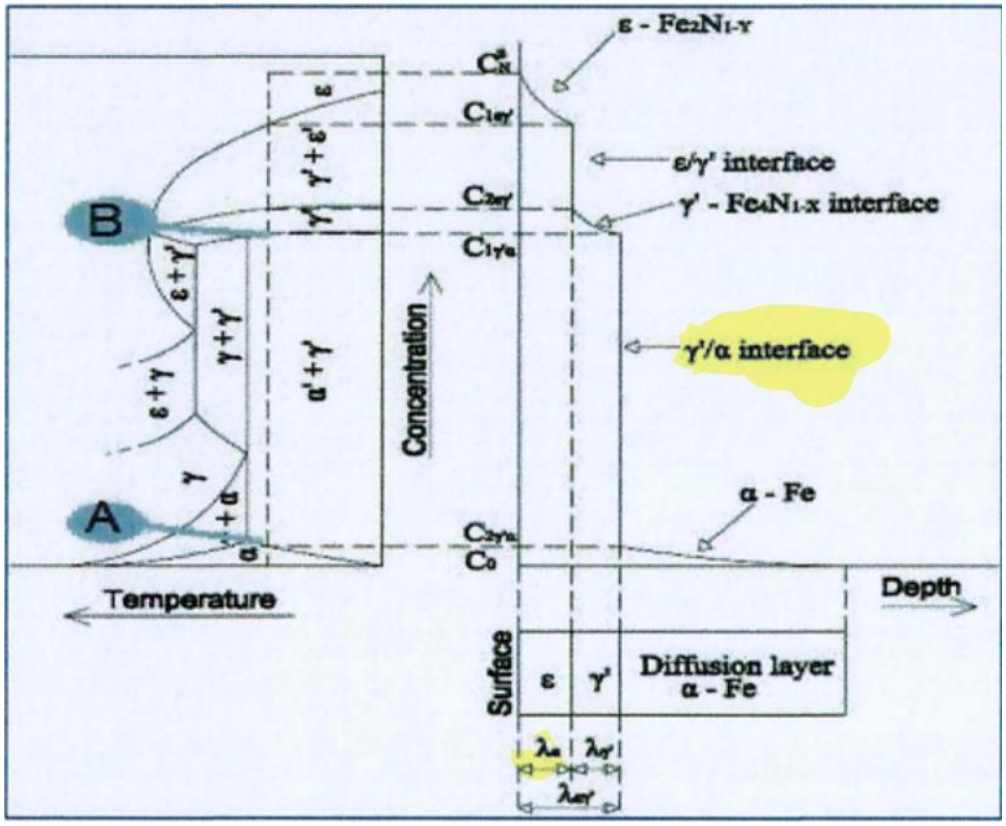

Figure 4.2. 1: Correspondence of phase diagram to nitriding surface

4.3 DICTRA Calculations for Cast Iron Nitriding

In the attempt to simulate the nitriding process in cast iron using DICTRA software, a small region of the surface needs to be set for the simulation to take place. This region should consist of α-ferritic phase and the rest of the phases found from thermodynamic calculations are to be dispersed into the ferrite. The results of the DICTRA simulation are predicted to present the nitrogen percentage that is diffused into this region through the nitriding process in relation to the region's width, as well as the amount of nitrides that are formed in the process and how much thickness will be achieved because of this nitride layer at the beginning of the region.

Firstly, using DICTRA's console mode, the nitriding simulation was run for the thesis' ductile cast iron with composition Fe-3.4wt%C- 4%Si- 1%Nb. Previously, the thermodynamic calculations took place for different contents of aluminum ranging from 0-4wt%. In order to easily push the nitriding process, the maximum Al content was used for the kinetic simulation (4wt%Al). The phase Si_3N_4 was once again suspended since it was not visible in the experimental data. As shown in ***Figure 3.2. 13***: Composition of alloying elements in BCC (α) phase- 4%Al- 510◦C***Figure 3.2. 13*** the percentage of Nb inside the ferritic phase is almost non-existent, so the Nb alloy was ignored during the computational process. The simulation ran under the following conditions:

1. Specific nitriding temperature was set at T=783K (510◦C).
2. For the nitrogen, gaseous phase was set as the reference state.
3. Nitrogen activity ACT(N)=100 was set as the lower boundary condition.
4. Alloying elements' contents in the ferritic phase were selected as such:
   3.4wt% and 4wt% are the alloy's contents in C and Al respectively and were selected to favor the cast iron's nitriding. The contents 5.16wt%Si and 0.028wt%N were selected because of thermodynamic data based on ***Figure 3.2. 12*** showing the composition of Si and N in BCC phase for a specific N percentage.

The phases retained for this calculation were the α-ferritic phase (BCC), γ'-nitride (Fe_4N), Graphite, Gas, AlN and ε-nitride phase (HCP). A ferritic region of 3e-3 width was set for the simulation and the phases γ', graphite, AlN and ε were entered into the region as dispersed phases. The simulation time was set to 50000 seconds (13 hrs. 53mins 20s) and 4 different times are presented in order to study the progress during nitriding: 100s, 1000s, 10000s and 20000s. In the figures below, the results of the simulation are shown. ***Figure 4.3. 1*** presents the weight percentage of nitrogen (x-axis) that is being diffused, and at which distance (m) from the material's outer surface (y-axis), in the times mentioned above. It is evident that as the time goes by the N percentage jumps to higher values, which is expected due to the constant N atom supply of the diffusion. However, this graph showcases that the nitrogen percentage calculated for each time stays constant (flat line) throughout the material. Additionally, in ***Figure 4.3. 2*** the amount of γ' phase (x-axis) in relation to the distance (y-axis) is presented. The γ' phase is all concentrated at the very beginning of the region and almost abruptly is minimized to zero for the entirety of the region (vertical lines) for each time calculated. The γ'-nitride percentage is increased for each time locally, once again due to the diffusion, without entering in deeper distance. Finally, in ***Figure 4.3. 3***, a flat line is visible concerning the amount of ε-nitride phase, which shows that this phase has not formed at all during the simulation time. All the above observations lead to the conclusion that these calculations result in incorrect kinetic data that do not logically correspond to the concept of the nitriding process.

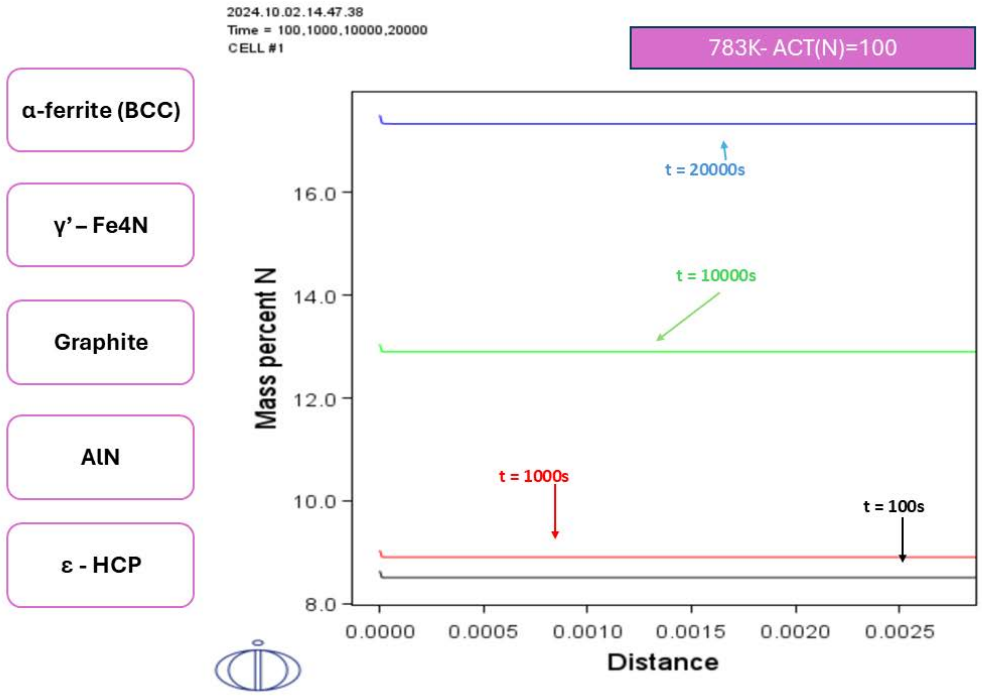

Figure 4.3. 1: Mass percentage of N (x-axis) / Distance into the surface (y-axis) [ACT(N)=100] [510◦C]

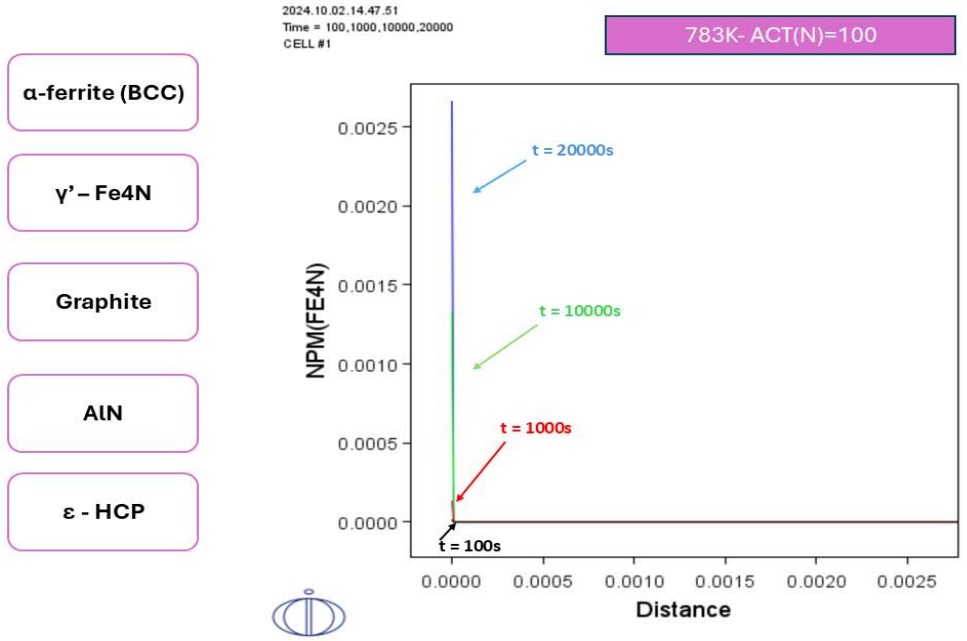

Figure 4.3. 2: Amount of γ' (x-axis) / Distance into the surface (y-axis) [ACT(N)=100] [510◦C]

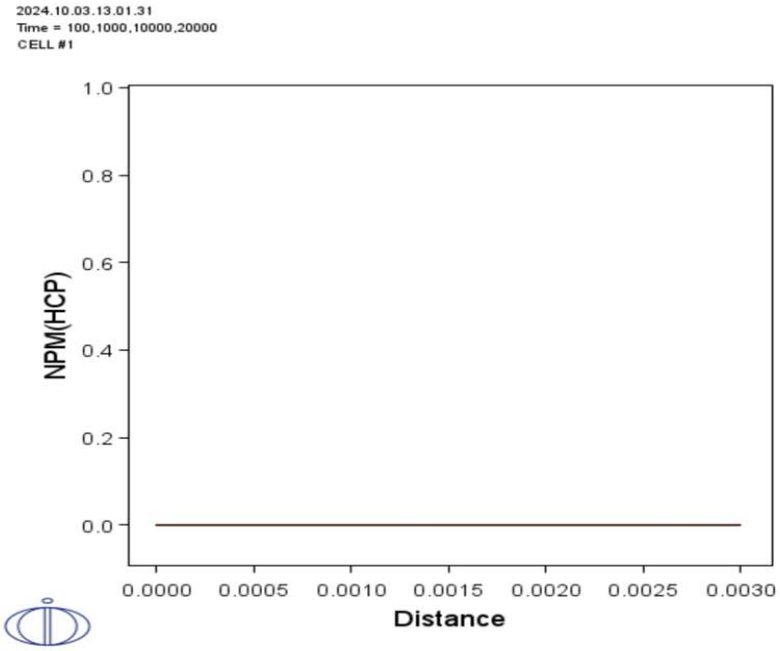

Figure 4.3. 3: Amount of ε (x-axis) / Distance into the surface [ACT(N)=100] [510◦C]

After these calculations that led to error, it was decided to repeat the simulation suspending phases AlN and ε-nitride. Therefore, a region of α-ferritic phase was entered and phases γ' and graphite were dispersed into the region. This region represents a part of the beginning of the diffusion zone on the cast iron's surface. For the nitriding simulations, the same conditions as before were used: T=783K (510◦C), gas was set as the reference state for N, simulation time set at 50000 seconds, ACT(N)=100. The compositions of the alloying elements into the α-phase were once again: 3.4wt%C, 4wt%Al, 5.16wt%Si, 0.028wt%N. The results of this simulation concerning the weight percentage of nitrogen are shown in ***Figure 4.3. 4***, for times 100s, 1000s, 10000s and 20000s. For each time, the N percentage follows a path while entering deeper into the region.

- ***100 seconds***: At this point the percentage of nitrogen right on the outside of the surface is ***5.84wt%*** and very early into the region reaches ***7.38wt%*** at distance 9.8e-6. This N value, which is the maximum, stays constant until distance 1.7e-4 and finally a very slight decrease is evident from distance 1.7e-4 to 1.8e-4, where the N percentage is ***7.36wt%*** and remains so for the rest of the region.
- ***1000 seconds***: As the N diffusion continues, the initial N percentage at that time has increased to ***6.16wt%*** and reaches maximum value of ***7.67wt%*** at the same distance of 9.8e-6 into the region, remaining constant until distance 8.4e-5. After this point, a downhill decrease of the percentage begins that finally settles at ***7.5wt%*** at distance 2.1e-4 for the rest of the region.

- ***10000 seconds***: At this point, the initial increase of N begins from ***10.3wt%*** and reaches ***10.54wt%*** at distance 9.8e-6. The percentage is constant until the nitrogen reaches the distance 7.3e-5 in the region. Then a more abrupt decrease of the percentage occurs until distance 1.8e-4 at ***9.4wt%.*** After a small increase at ***9.6wt%*** at distance 2.2e-4, a gradual decrease begins again that continues until the end of the region where the N percentage is settled at ***8.7wt%.***
- ***20000 seconds:*** At the final time, the initial increase of N begins from ***12.8wt%*** and reaches ***13.73wt%*** at the same region distance of 9.8e-6. The nitrogen once again remains constant until distance 7.3e-5. A similar path is followed as the time of 10000s with the abrupt decrease ending at ***11.4wt%***, at the same distance 1.8e-4. It increases slightly and reaches ***11.9wt%*** at the same distance 2.2e-4. Finally, the N gradually decreases, and its value is noted as ***10.2wt%*** at the end of the region.

In the two final calculations for 10000s and 20000s, a very similar path is observed. In both cases, at distance ranging from 7.3e-5 to 1.8e-4, the abrupt decrease of N percentage is not gradual, but the percentage fluctuates , decreasing, increasing a little bit and then decreasing again to the minimum value until the distance 1.8e-4, where the γ' phase stops being formed (shown in ***Figure 4.3. 6***). Due to this, the simulation appears unstable, since the desired results would include gradual, smooth decrease of N along the inside of the region.

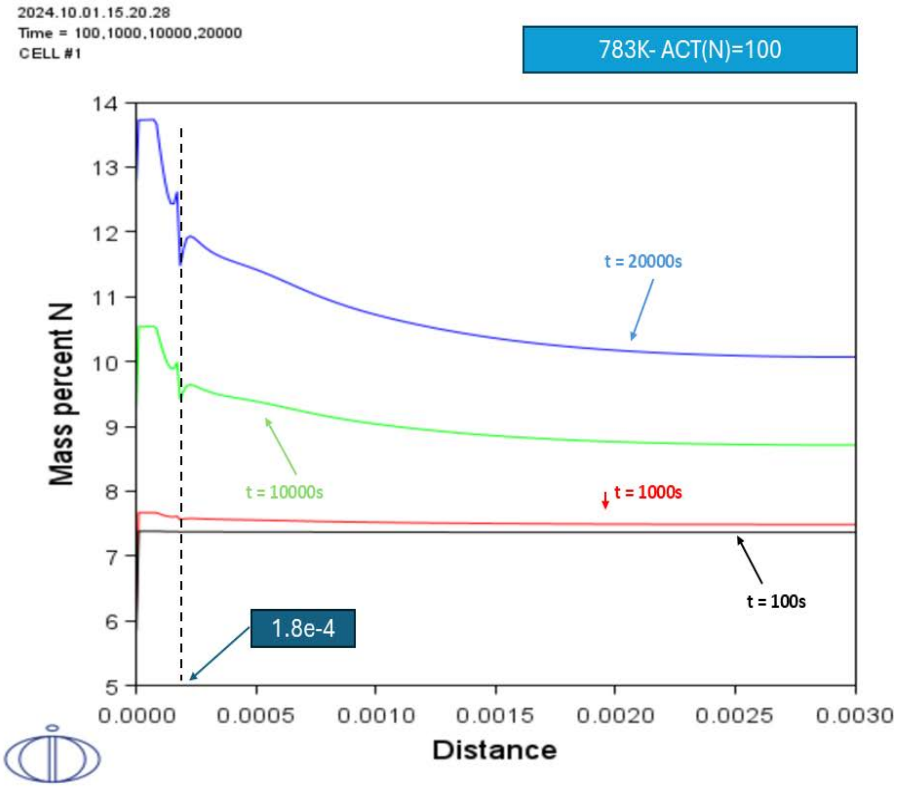

Figure 4.3. 4:Mass Percentage of N (x-axis) / Distance into the surface (y-axis) [ACT(N)=100] [510◦C]

The amount of each phase at the different times is presented in ***Figure 4.3. 5***. At the top of the graph the α-ferritic phase is visibly increasing with the diffusion from ***62 wt%*** to ***68wt%*** at the beginning of the region and stabilizing at distance 1.8e-4 into the region, reaching the highest value for 20000 seconds at ***75 wt%.*** In the middle of the graph, the graphite phase is mostly constant throughout the region, increasing along with the diffusion from ***24wt%*** at 100s to ***36wt%*** at 20000s. Finally, ***Figure 4.3. 6*** concentrates on the γ' phase, zooming at the bottom part of the previous figure in order to clearly demonstrate the γ' path at the different points of the simulation. For each time, it is noted that the maximum distance γ' achieves inside the region is 1.8e-4. However, in the distance range of 1.4e-4 to 1.5e-4 a flat line is noted, where γ'-phase does not form. Right after this gap abrupt triangles of phase γ' are formed until distance 1.8e-4. This behavior exhibits instabilities in the calculations, confirming what was mentioned above.

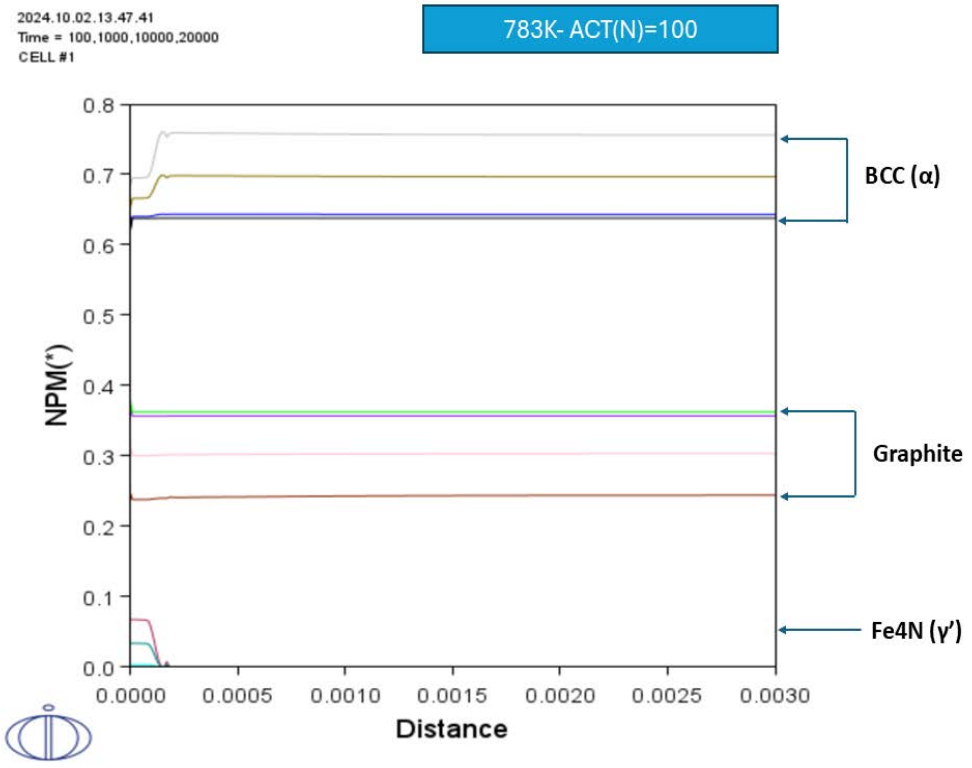

Figure 4.3. 5:Amount of all phases (x-axis) / Distance into the surface [ACT(N)=100] [510◦C]

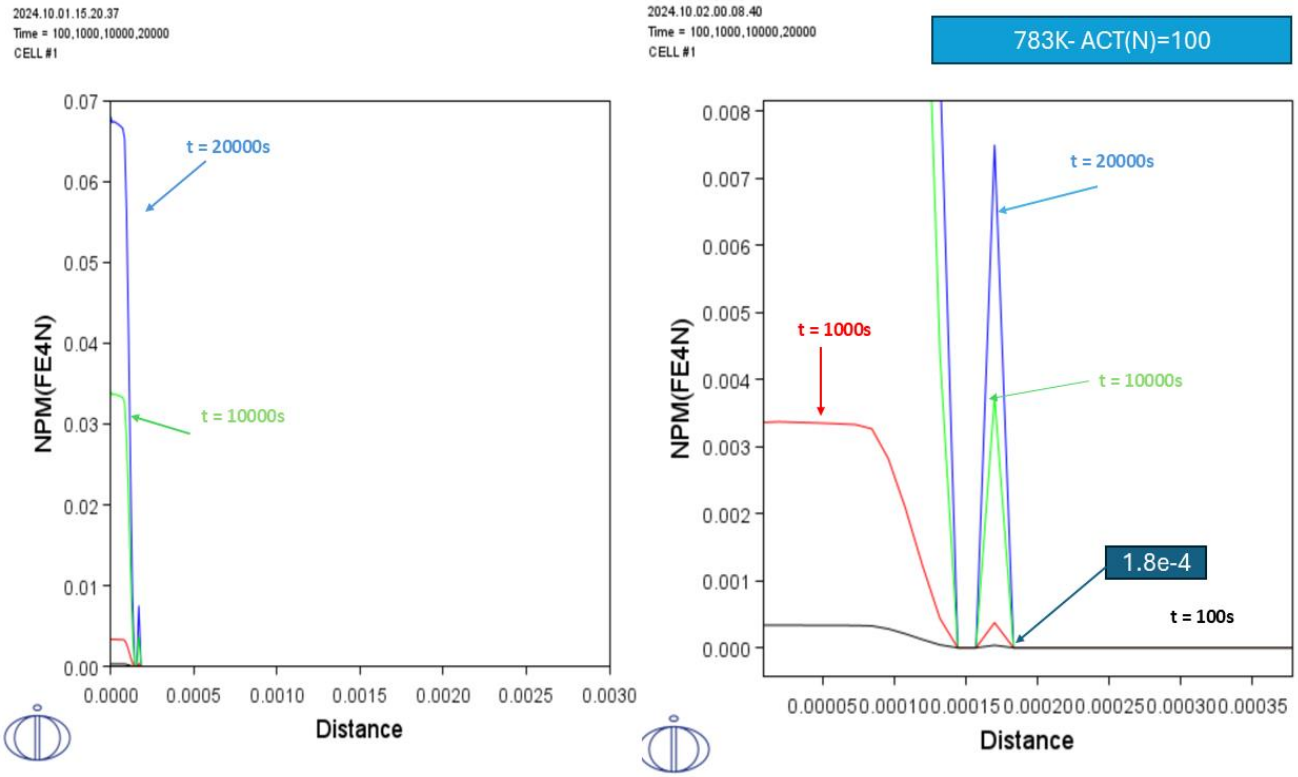

*Figure 4.3. 6:*Amount of γ' (x-axis) / Distance into the surface (y-axis) [ACT(N)=100] [510◦C]

4.4 Nitriding Simulations (DICTRA) for N Activity: 1000 & 3000

The next step in this thesis, was to study the effect of higher nitrogen activity as the problem's lower boundary. The same simulations were run, setting ACT(N)=1000 and ACT(N)=3000, with the goal of achieving smoother and more gradual entrance of Nitrogen and γ'-nitride phase into the studied ferritic region.

Therefore, the calculations were performed for alloy contents: 3.4wt%C, 4wt%Al, 0.0028wt%N, 5.16wt%N. The nitriding temperature remained at T=783K (510◦C) and the simulation ran for 50000 seconds. The gaseous phase was set as the reference state for the nitrogen.

The activity of nitrogen was set as the lower boundary condition at:

A) ACT(N) = 1000

B) ACTN(N) = 3000

A) The results of the first nitriding simulation can be shown in the following figures. ***Figure 4.4. 1*** presents the N percentage that is diffused into the region during the process for times: 100s, 1000s, 10000s and 20000s. For the first two time points, the N percentage seems to remain mostly constant through the whole region at ***7.36wt%*** and ***7.5wt%*** respectively. For the other two calculations, the nitrogen percentage firstly increases until the maximum value and after some distance inside the region, gradually decreases until the settled value at the end of the region. Those values are presented in ***Table 4.4. 1*** below:

Table 4.4. 1: 10000s & 20000s

	Initial %	**Max %, Distance**	**Final %**
10000s	10.2wt%	10.8wt%, 1.3e-4	8.8wt%
20000s	13.1wt%	13.5wt%, 1.3e-4	10.2wt%

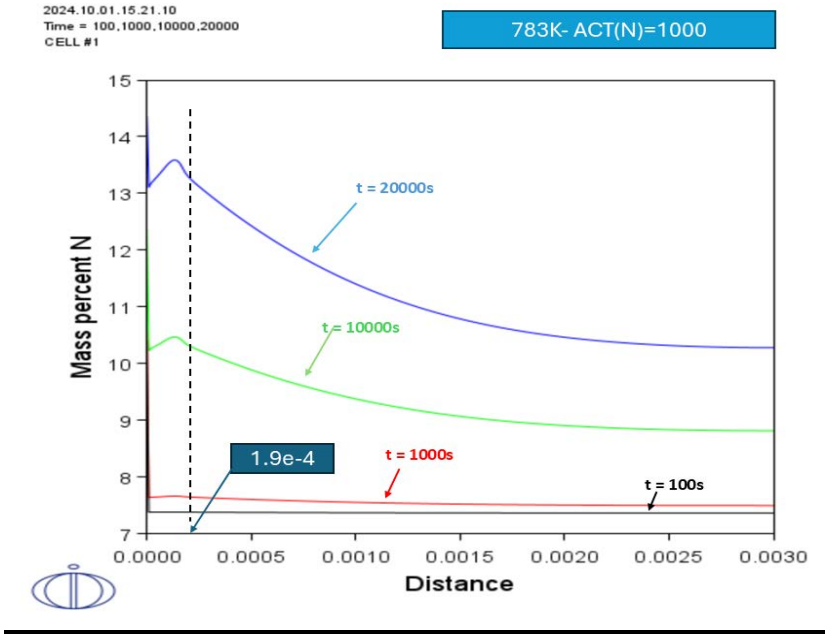

Figure 4.4. 1: Mass Percentage of N (x-axis) / Distance into the surface (y-axis) [ACT(N)=1000] [510◦C]

Comparing this result with the results of ***Figure 4.3. 4*** it can be noted that the final nitrogen percentages at the end of the region are the same for both cases. However, the lines in the second figure don't exhibit any instabilities and the percentage gradually decreases as the N is diffused into the region. Two more differences between the ACT(N)=100 and ACT(N)=1000 can be observed by comparing ***Figure 4.4. 2*** to ***Figure 4.3. 6***, both showcasing the formation of γ' inside the region. In this case it can once again be noted that no simulation instabilities are evident, since for each time calculation the amount of γ' decreases from its initial value at the beginning of the region without exhibiting any anomaly and stops forming at distance 1.9e-4. Therefore, the higher activity 1000 makes the γ' form until slightly further into the region. Finally, it can be observed that for nitrogen activity 1000, the region is richer in γ'-nitrides since the maximum value of each time exceeds the ones from the previous calculation.

Max γ' percentage for:

- **100s**: 0.035% for activity 100 → 0.06% for activity 1000
- **1000s**: 0.34% for activity 100 → 0.61% for activity 1000
- **10000s**: 3.4% for activity 100 → 6.1% for activity 1000
- **20000s**: 6.8% for activity 100 → 12.2% for activity 1000

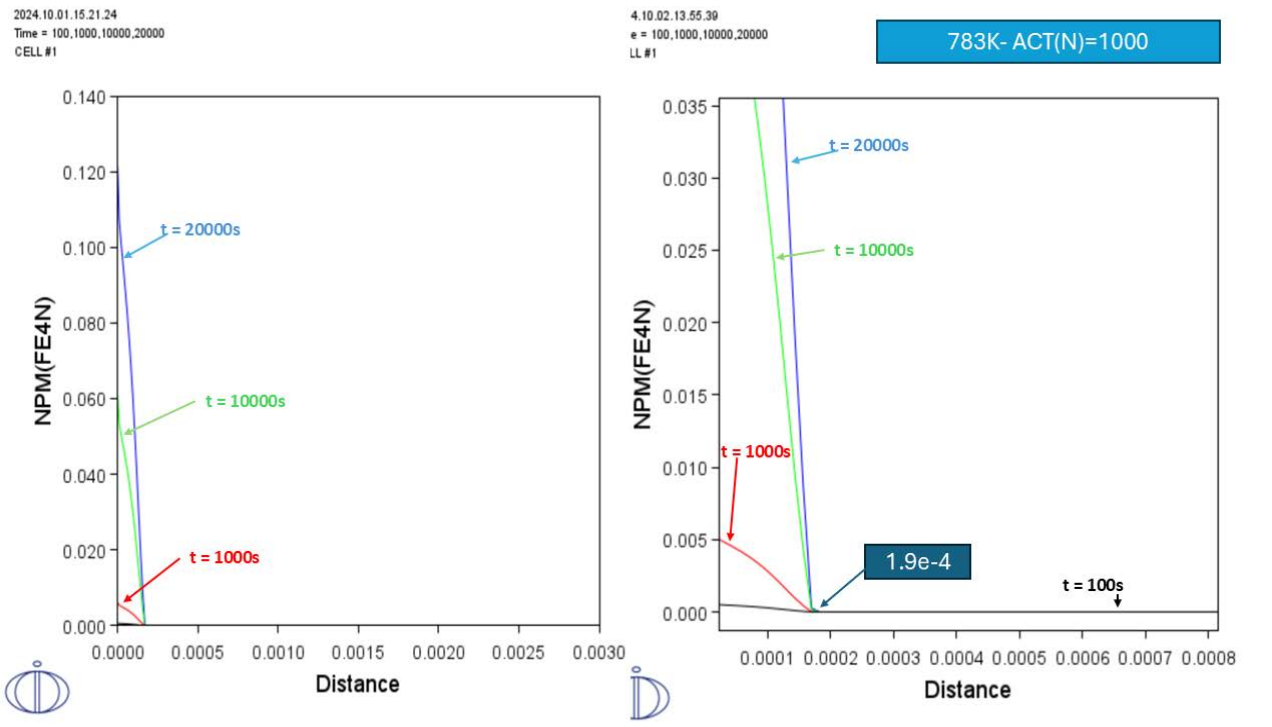

Figure 4.4. 2: Amount of γ' (x-axis) / Distance into the surface (y-axis) [ACT(N)=1000] [510◦C]

B) Similarly, the results for ACT(N)=3000 can be studied in ***Figure 4.4. 3*** and ***Figure 4.4. 4***. For the first graph the difference that is observed comparing to the activity 1000, is that for times 10000s and 20000s, two similar "summits" seem to form for the nitrogen percentage before its gradual decrease. The final values of N at the end of the region appear to be slightly higher in comparison to ***Figure 4.4. 1*** at ***8.9wt%*** and ***10.3wt%*** respectively. Even though when comparing the amount of γ'-nitrides for N activity 3000 to the previous calculation there is a decrease in the percentage formed, it observed that the distance in which the nitrides reach inside the region is higher, reaching 3e-4 from 1.9e-4 on the previous case.

Max γ' percentage for:

- **100s**: 0.035% for activity 100 → 0.06% for activity 1000→ 0.06% for activity 3000
- **1000s**: 0.34% for activity 100 → 0.61% for activity 1000→ 0.53% for activity 3000
- **10000s**: 3.4% for activity 100 → 6.1% for activity 1000→ 5.4% for activity 3000
- **20000s**: 6.8% for activity 100 → 12.2% for activity 1000→ 10.8% for activity 3000

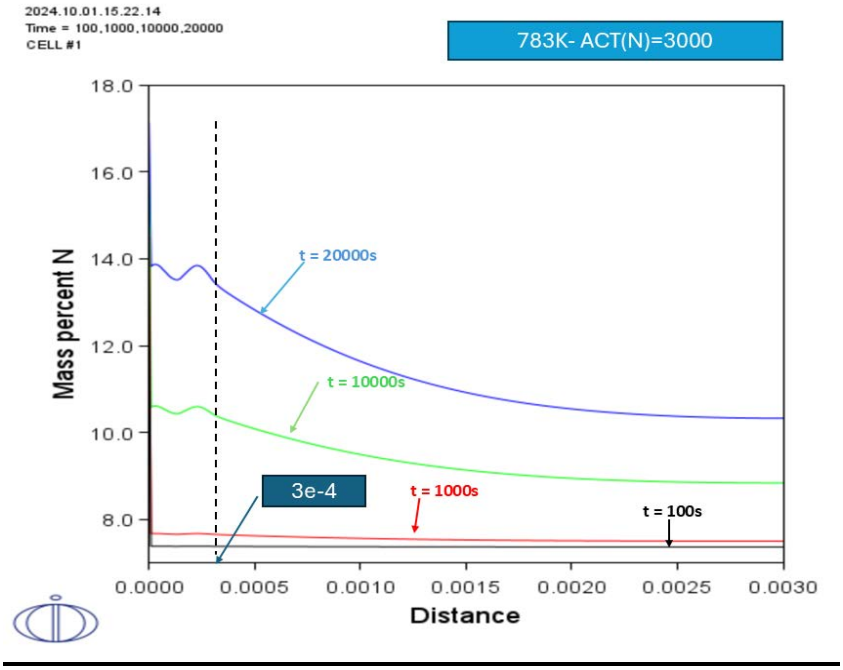

Figure 4.4. 3: Mass Percentage of N (x-axis) / Distance into the surface (y-axis) [ACT(N)=3000] [510◦C]

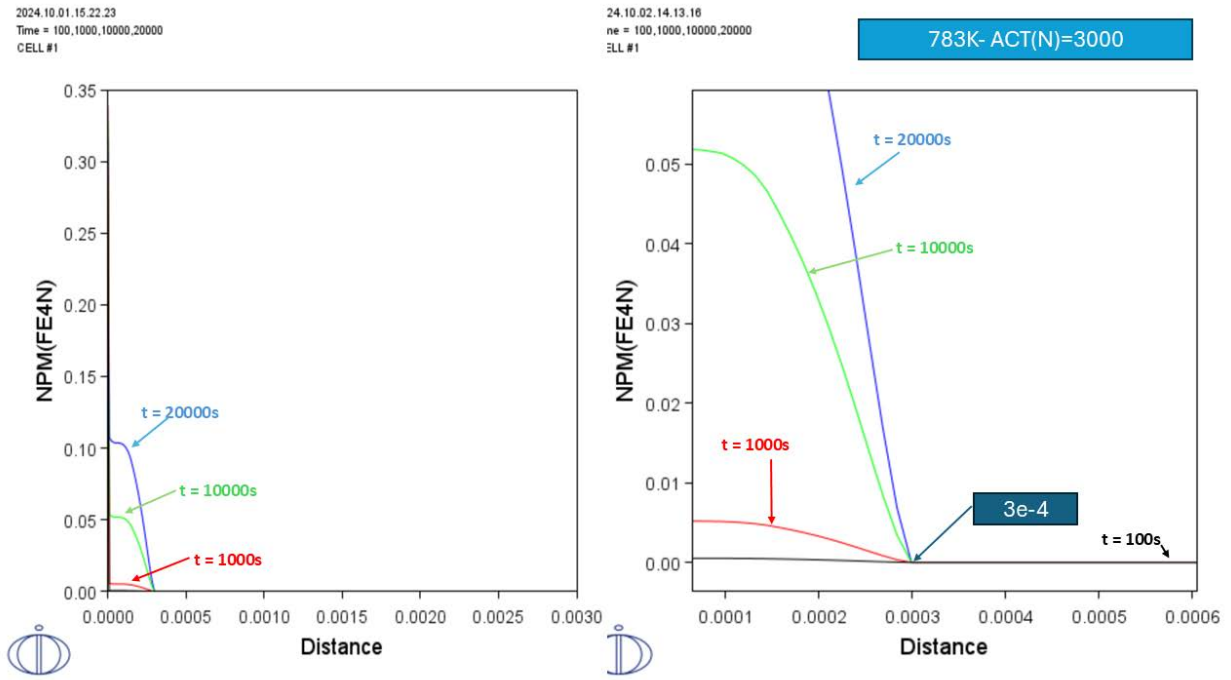

Figure 4.4. 4: Amount of γ' (x-axis) / Distance into the surface (y-axis) [ACT(N)=3000] [510◦C]

The results from these 3 calculations and the comparison between is presented in ***Figure 4.4. 5*** and ***Figure 4.4. 6*** below, for 10000s and 20000s. This leads to the following conclusions about the increase of Nitrogen activity at nitriding simulations in this theses' cast iron:

- For higher N activity the formation of γ' nitrides are enhanced and are formed in a more stable manner and at higher percentage into the material's surface.
- Higher N activity causes nitrogen to penetrate deeper into the material over a given period, resulting in a thicker γ'-nitride layer.
- Nitrogen activity is a controllable factor which can be set at a specific value in order to favor the formation of the appropriate nitrides in order to achieve the desired material properties. Higher nitrogen activity levels favor the formation of γ'-nitrides (Fe_4N) which contribute to increased surface hardness of the cast iron.

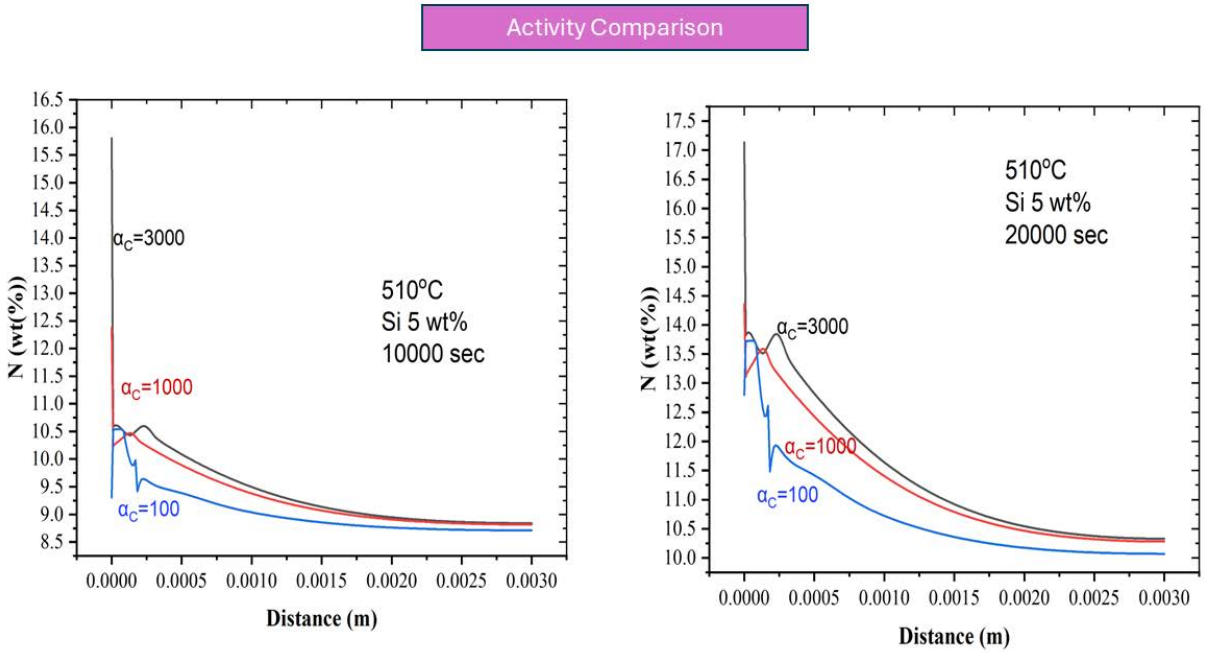

Figure 4.4. 5: Activity Comparison (N wt%) for 10000s & 20000s

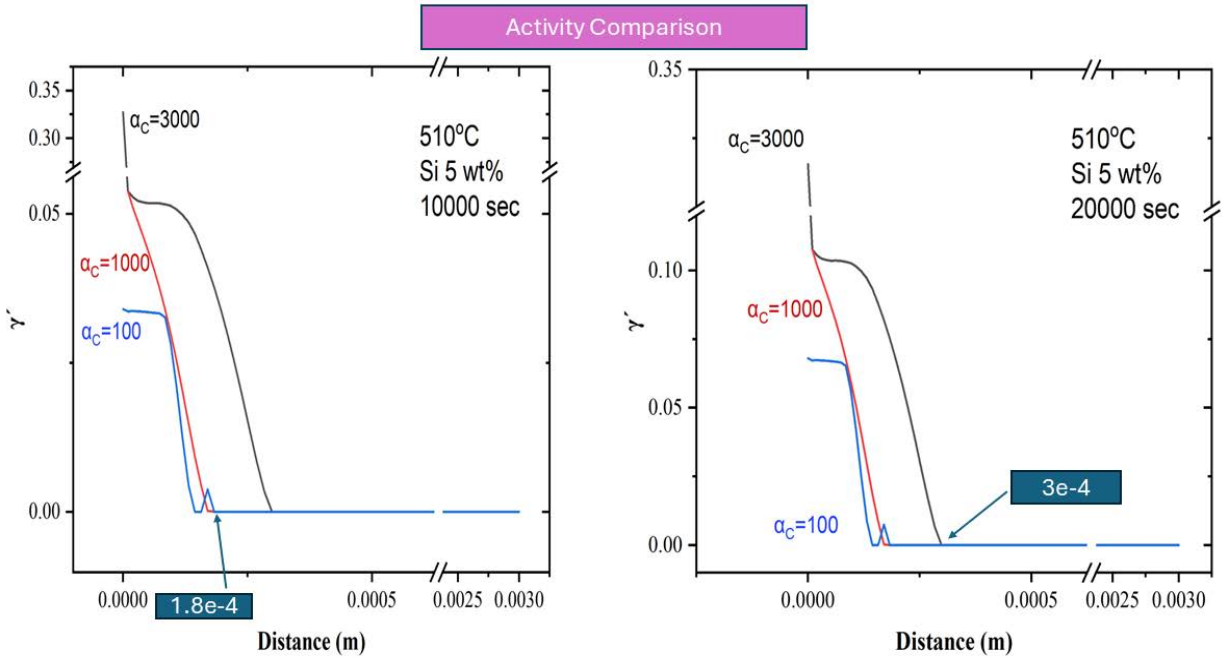

Figure 4.4. 6: Activity Comparison (γ') for 10000s & 20000s

4.5 Nitriding Simulations at 793K (520◦C)

As the next step for this thesis, it was decided to repeat the same simulations for a 10◦C higher nitriding temperature, at 793K (520◦C). The goal is to study the effect this temperature might have on the simulation results, the nitrogen diffusion and the nitride layer formation inside the studied designated region.

A. First, the simulation ran for ACT(N)=1000 lower boundary condition, for 50000 seconds. ***Figure 4.5. 1*** is compared to ***Figure 4.4. 1*** in order to examine the difference in N percentage during the simulation. It is evident that generally the paths that the nitrogen percentage follows throughout the region are somewhat similar. However, at the higher temperature simulation, the range that was previously unstable at 783K is now presented as a more gradual decrease of N. The instabilities of this distance now seem to have smoothed out. In addition, for each time (100s, 1000s, 10000s, 20000s) of the 520◦C simulation, the amount of nitrogen reaches deeper into the distance before beginning to decrease in comparison to the previous calculation. At temperature **793K** the decrease starts at distance **1.2e-4**, when at temperature **783K** the decrease starts at distance **7.3e-5**. In both cases the N percentage settles gradually at the end of the region at the same values. This comparison is shown in ***Figure 4.5. 2***.

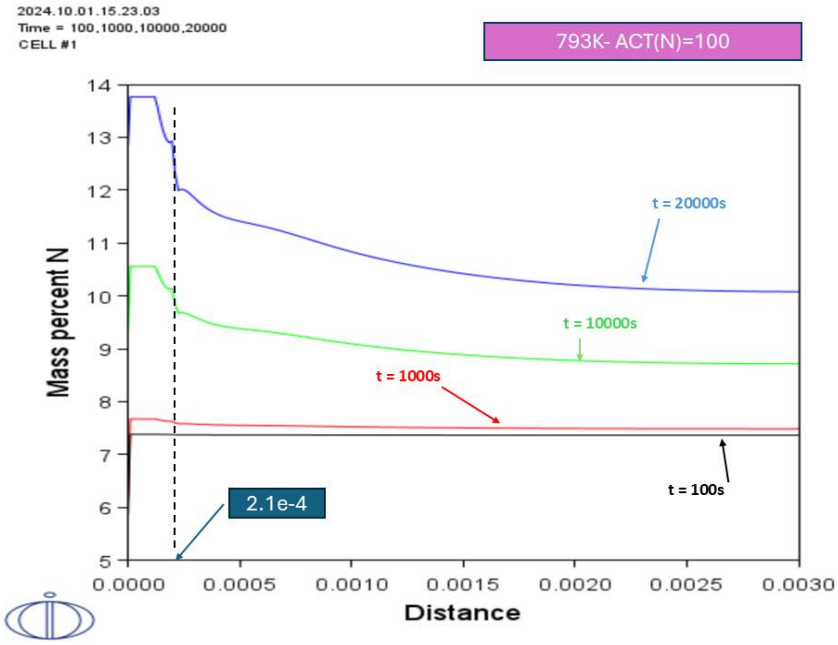

Figure 4.5. 1: Mass Percentage of N (x-axis) / Distance into the surface (y-axis) [ACT(N)=100] [**520◦C**]

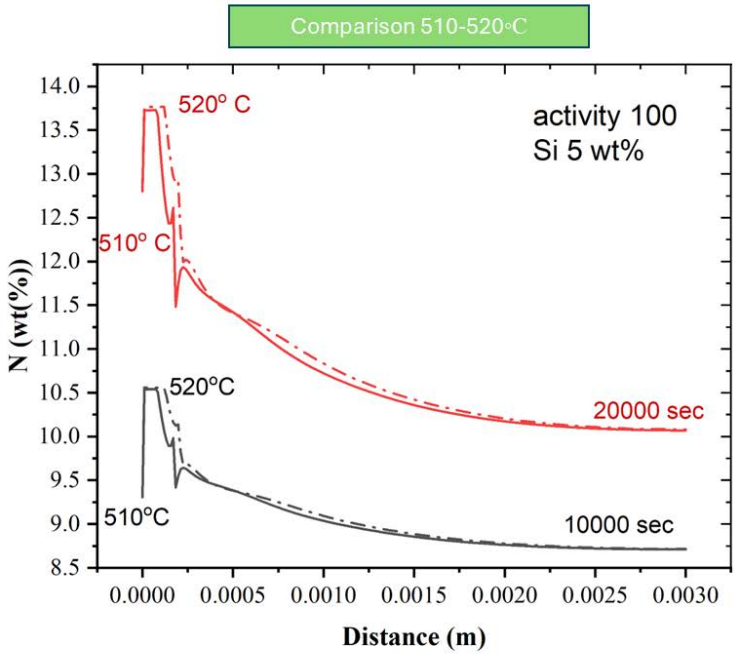

Figure 4.5. 2: Comparison of Nwt% / Distance between temperatures 510◦C and 520◦C [ac=100]

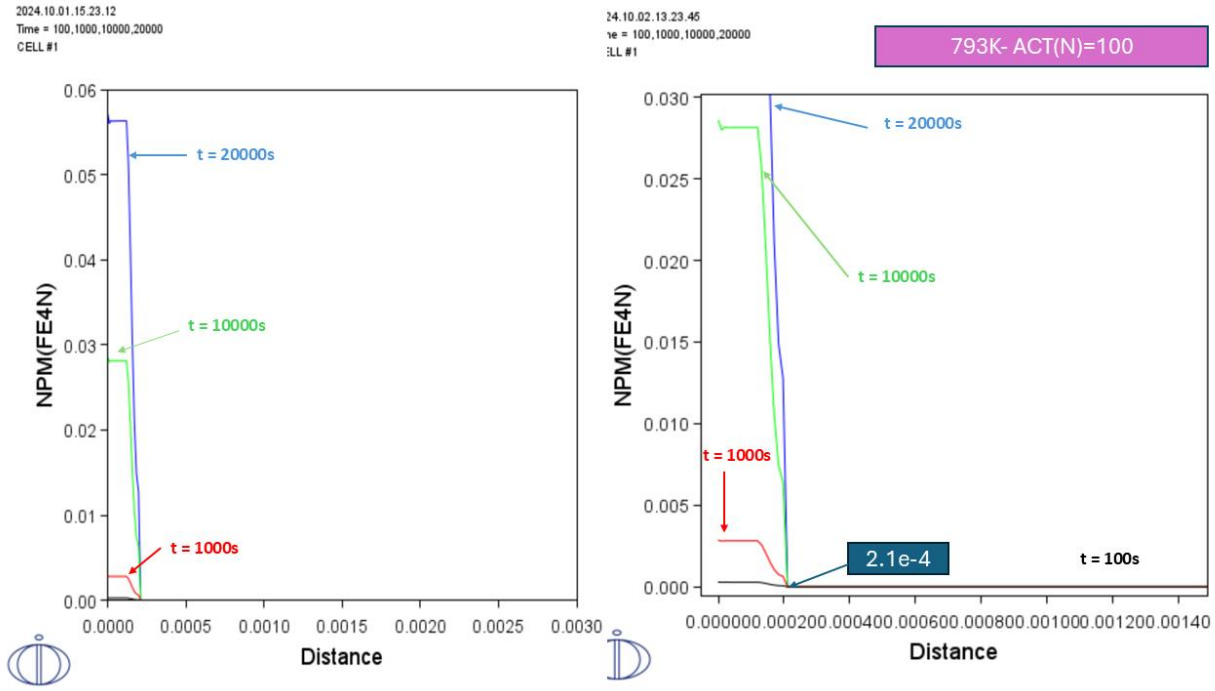

Figure 4.5. 3: Amount of γ' (x-axis) / Distance into the surface (y-axis) [ACT(N)=100] [**520◦C**]

The comparison of ***Figure 4.4. 2*** to ***Figure 4.5. 3*** concerning the formation of γ'-nitrides is presented in ***Figure 4.5. 4*** for 10000s and 20000s. It is noticeable that for the higher temperature simulation, the nitride layer penetrates deeper into the region at distance **2.1e-4** as opposed to distance 1.8e-4 at the lower nitriding temperature. On the other hand, even though at 783K a bigger γ' percentage is initially formed, instabilities are visible while entering the surface, which are not exhibited at 793K.

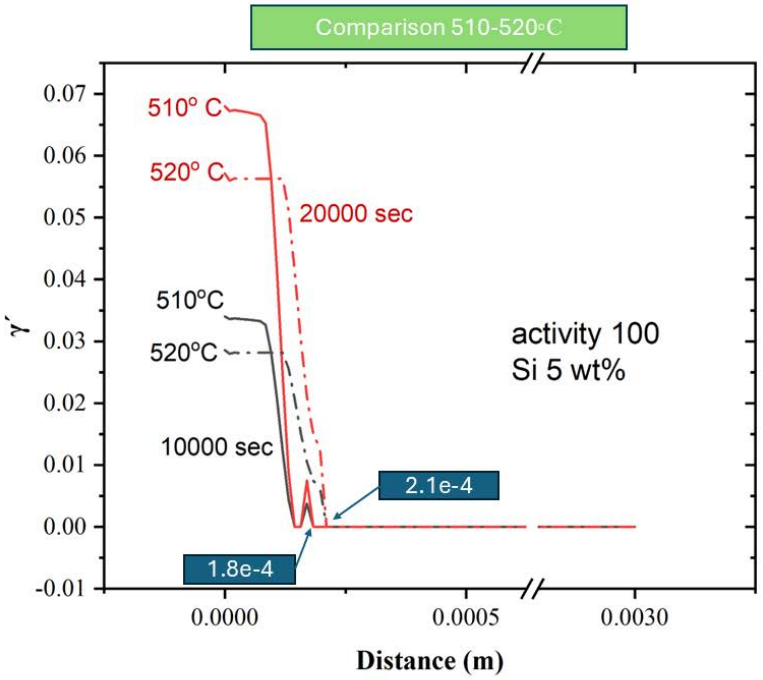

Figure 4.5. 4: Comparison of γ' / Distance between temperatures 510◦C and 520◦C [ac=100]

B. The N activity is now increased at 1000, and the nitriding simulation is performed once again. ***Figure 4.5. 3*** presents the percentage of nitrogen in relation to the distance inside the region and is compared to ***Figure 4.4. 1***. It seems that the maximum N percentage before the decrease is now higher at temperature **793K** than 783K for times 10000s and 20000s, **10.6wt%** and **13.8wt%** respectively. A slight increase is also visible for the value that the N percentage settles at the end of the region, at **8.9wt%** and **10.4wt%.** This comparison is presented in ***Figure 4.5. 6*** for 10000s and 20000s.

In addition, the comparison between ***Figure 4.5. 4*** at 793K and ***Figure 4.4. 2*** at 783K presented in shows that the γ' nitride layer stops at the same distance (1.8e-4) for both nitriding temperatures, however the amount of γ' formed at the start of the region seems to be decrease at higher temperature, from **12.1%** to **10.7%.**

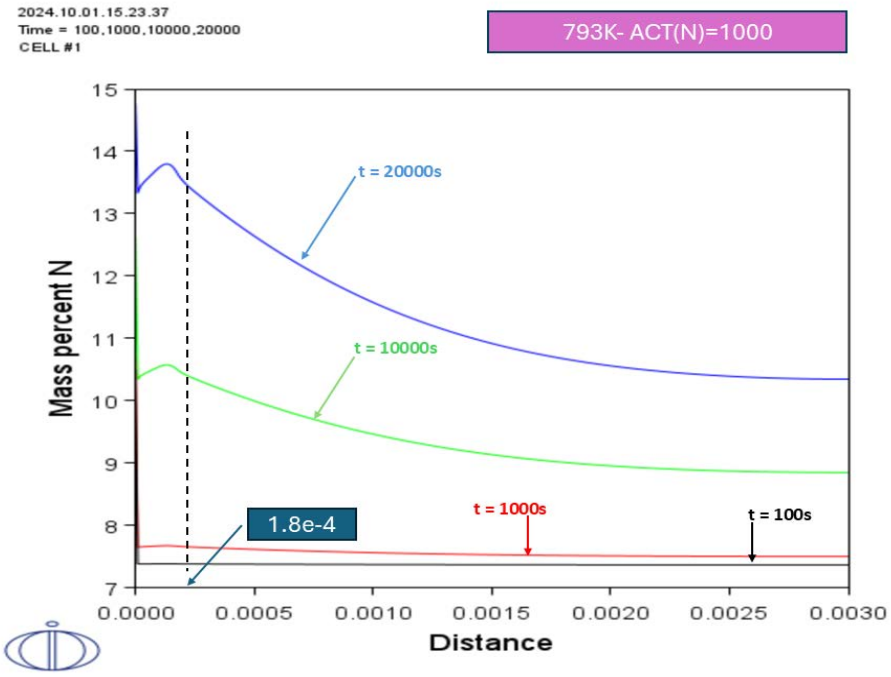

Figure 4.5. 5: Mass Percentage of N (x-axis) / Distance into the surface (y-axis) [ACT(N)=1000] [520◦C]

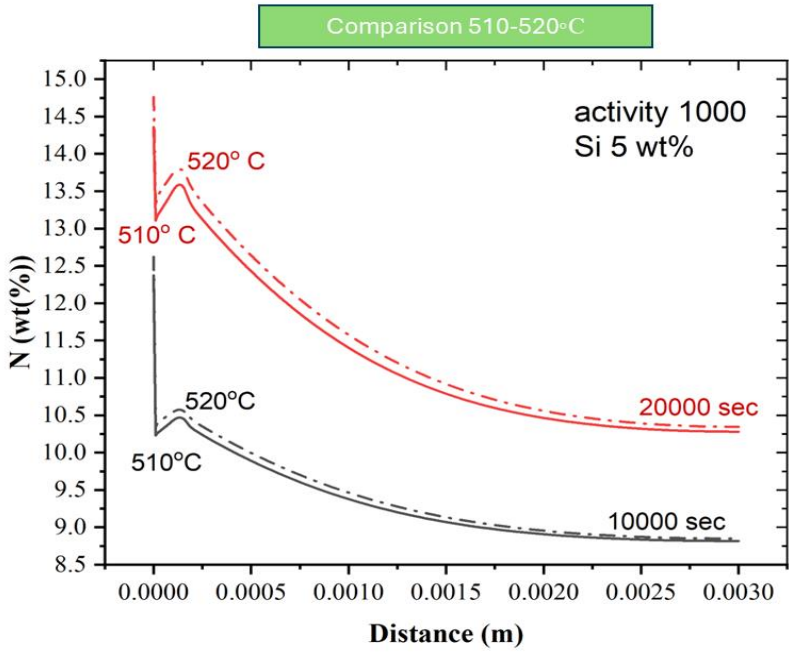

Figure 4.5. 6: Comparison of Nwt% / Distance between temperatures 510◦C and 520◦C [ac=1000]

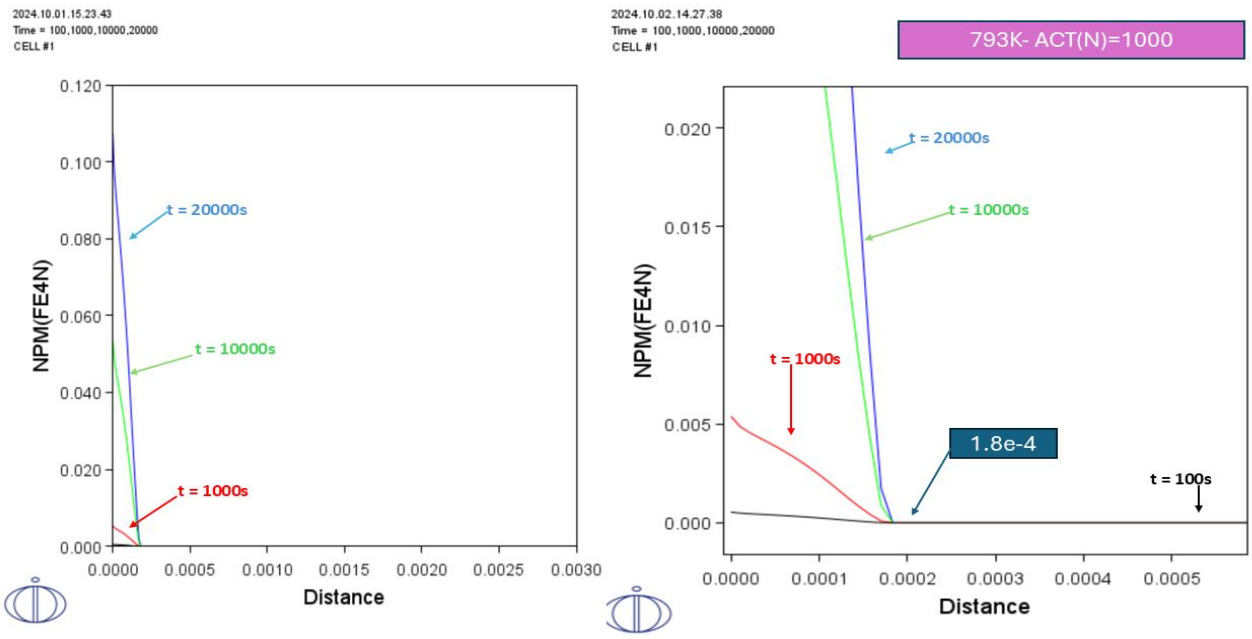

Figure 4.5. 7: Amount of γ' (x-axis) / Distance into the surface (y-axis) [ACT(N)=1000] [520◦C]

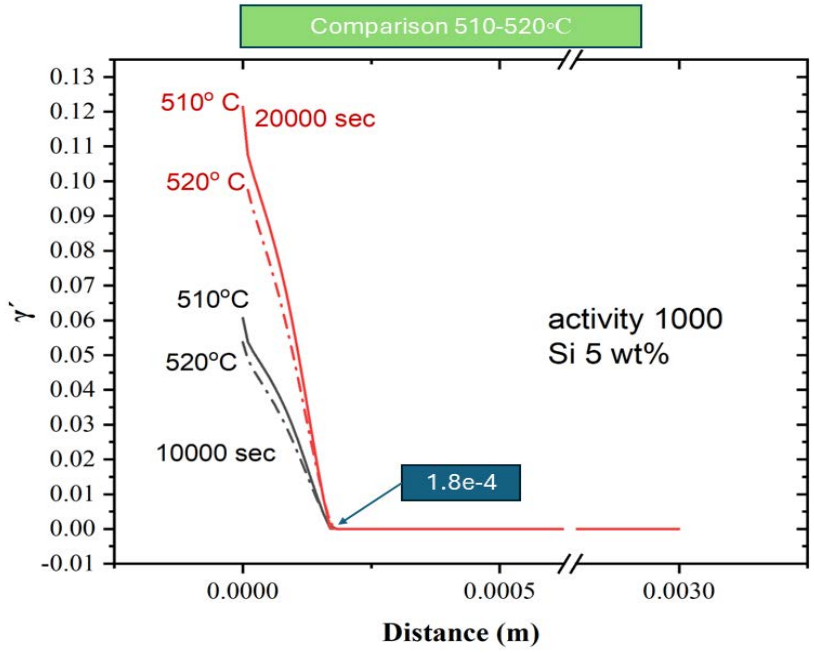

Figure 4.5. 8: Comparison of γ' / Distance between temperatures 510◦C and 520◦C [ac=1000]

C. For the next simulation the nitrogen activity is set even higher at ACT(N)=3000 in order to compare with ***Figure 4.4. 3*** and ***Figure 4.4. 4***. This comparison is visible in ***Figure 4.5. 10***. It is once again evident that the paths created by the nitrogen inside the region are increased in percentage, this time for all times calculated. The maximum nitrogen percentage from ***13.8wt%*** increases with the temperature at ***14.1wt%*** and the final N amount at the end of the region also increases from ***10.3wt%*** to ***10.5wt%*** at 20000 seconds.

When it comes to γ'-nitride percentage the comparison of the two simulations is presented in ***Figure 4.5. 6***. For both temperatures it seems that right at the beginning of the region, the initial value of γ' instantly decreases. At temperature 793K the nitride amount is lower than at the cast iron's nitriding temperature (783K). After that point the γ' percentage decreases gradually and reaches deeper into the region at the higher temperature, at 3.3e-4, as opposed to 3e-4 at 783K.

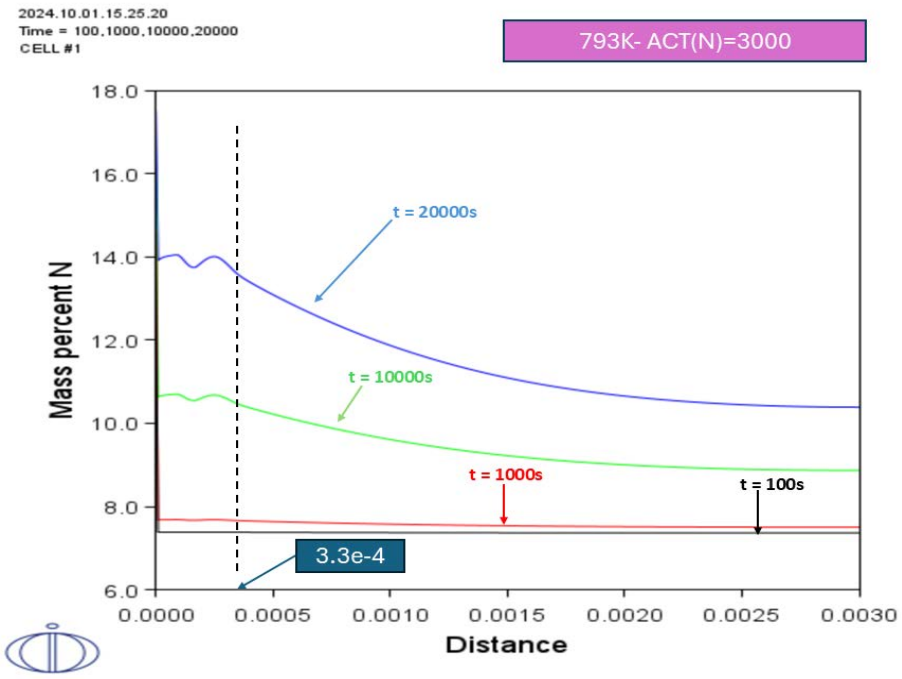

Figure 4.5. 9: Mass Percentage of N (x-axis) / Distance into the surface (y-axis) [ACT(N)=3000] [**520◦C**]

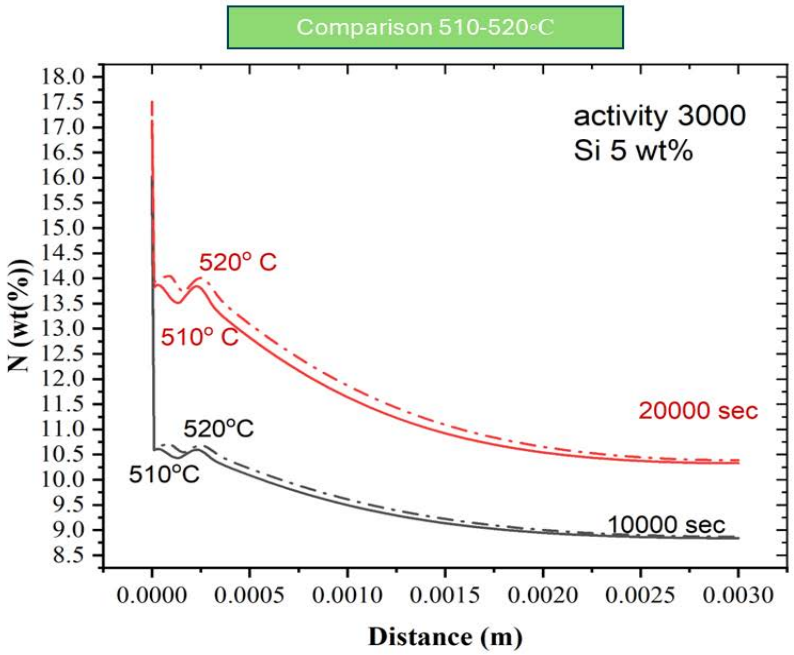

Figure 4.5. 10: Comparison of Nwt% / Distance between temperatures 510◦C and 520◦C [ac=3000]

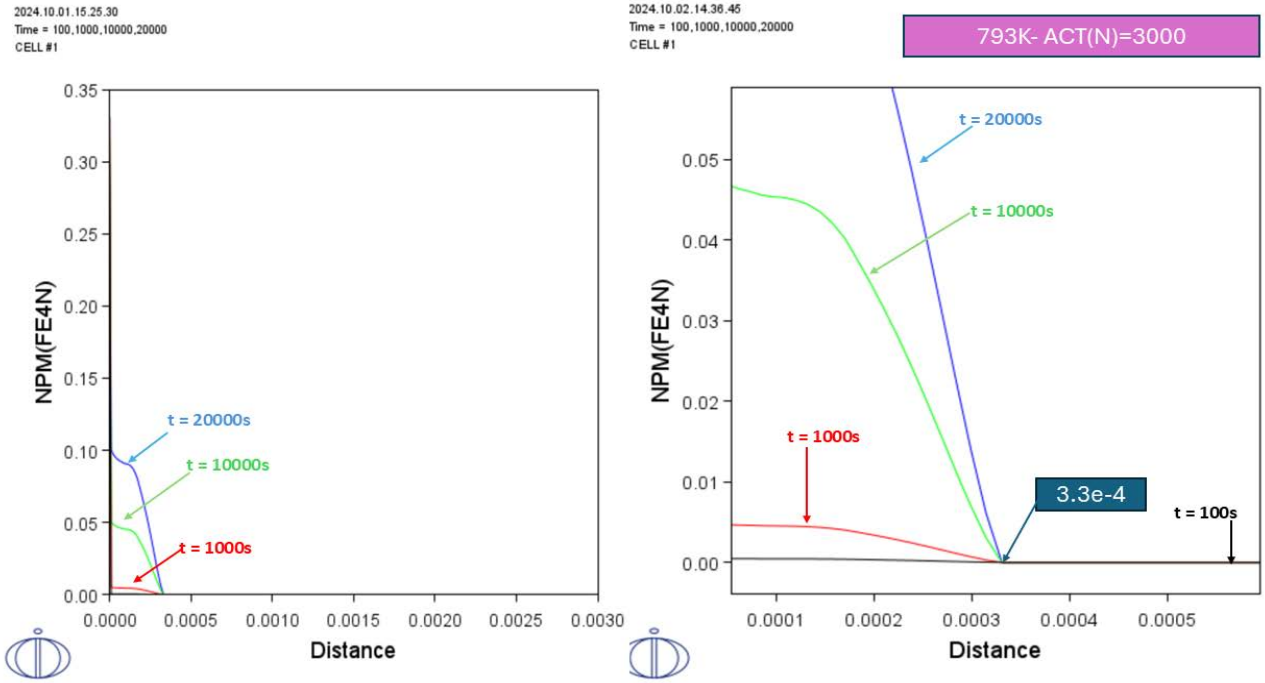

Figure 4.5. 11: Amount of γ' (x-axis) / Distance into the surface (y-axis) [ACT(N)=3000] [520◦C]

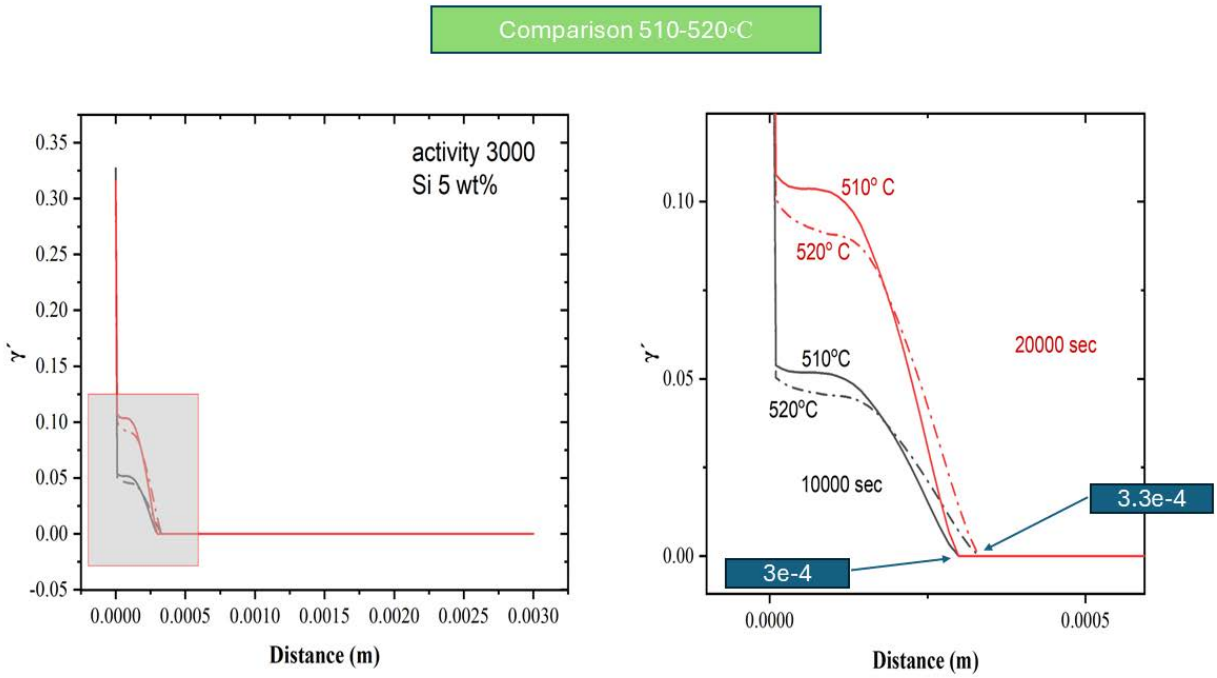

Figure 4.5. 12: Comparison of γ' / Distance between temperatures 510◦C and 520◦C [ac=3000]

The simulations that were performed at higher nitriding temperature 793K for different nitrogen activities lead to the following conclusion for this thesis' cast iron:

- For lower nitrogen activity 100, the 10-degree temperature increase helps the nitriding process not exhibit any instabilities as the diffusion of N atoms reaches deeper into the iron's surface. At the same time, the γ'-nitrides are able to gradually penetrate deeper into the surface region, creating a thicker nitride layer, providing more hardness to the surface [***Figure 4.5. 2***& ***Figure 4.5. 4***].
- For nitrogen activity 1000 at 793K, the nitrogen that is diffused into the surface increases, which is expected due to the higher nitrogen activity. However, in this case, the temperature increase does not allow the γ'-phase to reach any deeper into the region, which means that for the same nitride layer thickness as the lower temperature, this region's layer is not as rich in γ' as at 783K [***Figure 4.5. 6*** & ***Figure 4.5. 8***].
- For the highest nitrogen activity 3000, the 10-degree increase in temperature causes the N to be diffused in even higher percentages into the region, similar to the 1000 activity simulation. The γ'-nitride amount slightly decreases at 793K, but this time the nitrides are allowed to form a bit deeper into the region, adding thickness to the layer [***Figure 4.5. 10*** & ***Figure 4.5. 12***].

4.6 DICTRA Calculations for 4wt%Si & ACT(N)=1000- [510◦C]

After the simulations that were performed, the interest of examining the effect of alloying element Si content was sparked. Therefore, it was decided to repeat this calculation for lower Si content, this time setting the ferritic region's composition as such: **3.4wt%C**, **4wt%Al**, **4wt%Si** and **0.0001wt%N**, which is the alloying composition of the studied cast iron. The nitriding temperature remains at 783K (510◦C), gaseous phase was set as the reference state for nitrogen and as mentioned, the N activity was set as the lower boundary condition at value of 1000, as the previous calculation's medium. However, the run time for this simulation was decided to be set higher, at 500000sec in order to study the nitriding simulation for a longer period of time. The percentage of nitrogen entering the ferritic region in relation to the depth it reaches for times: 50000s, 100000s, 150000s, 250000s and 500000s is visible in ***Figure 4.6. 1***.

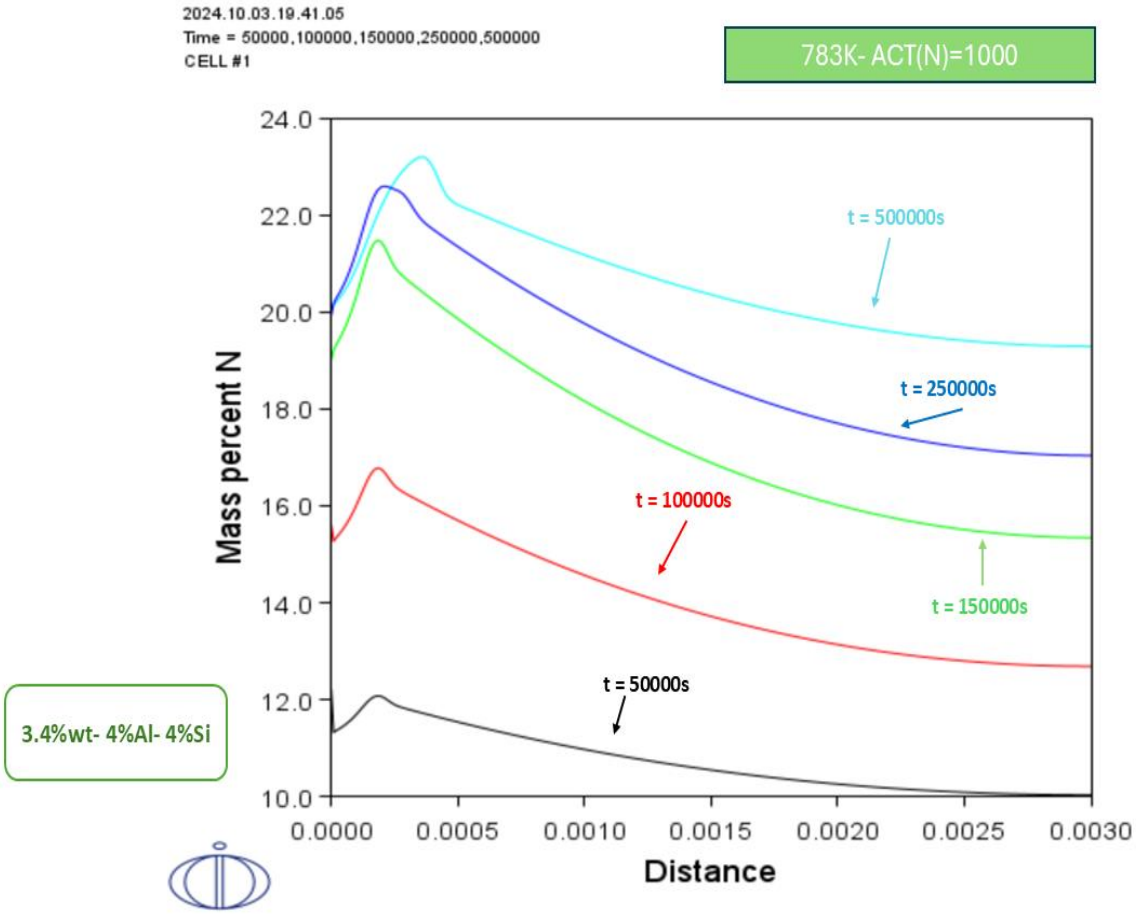

Figure 4.6. 1: Mass Percentage of N (x-axis) / Distance into the surface (y-axis) [ACT(N)=1000] [510◦C]

Like before, starting at the beginning of the region, the nitrogen percentage increases until the maximum value and then gradually decreases little by little until the end of the region, creating a summit-like shape with the highest nitrogen value as the top. At the end of the simulation, at 500000 seconds, the maximum N value is ***23.2wt%*** at distance 3.5e-4 inside the region. The amount of N gradually settles at ***19.3wt%*** at the end of the region. It is noted that for 50000 seconds, the maximum percentage reaches ***12.08wt%*** at distance 1.8e-4. ***Figure 4.4. 1*** shows that at the same distance at time 20000s < 50000s, the maximum N percentage reaches higher at ***12.2wt%.*** The basic difference in conditions between the two calculations is the content in Si alloying element. For the first calculation the content is **5.16wt%Si** while for the second it is lower, at **4wt%Si**. From this observation we can deduct the conclusion that the increase of Si content in cast irons during nitriding can cause the diffusion of N atoms into the material's surface to take place faster and higher nitrogen percentages are reached sooner. The comparison between the two simulations is evident in ***Figure 4.6. 2***.

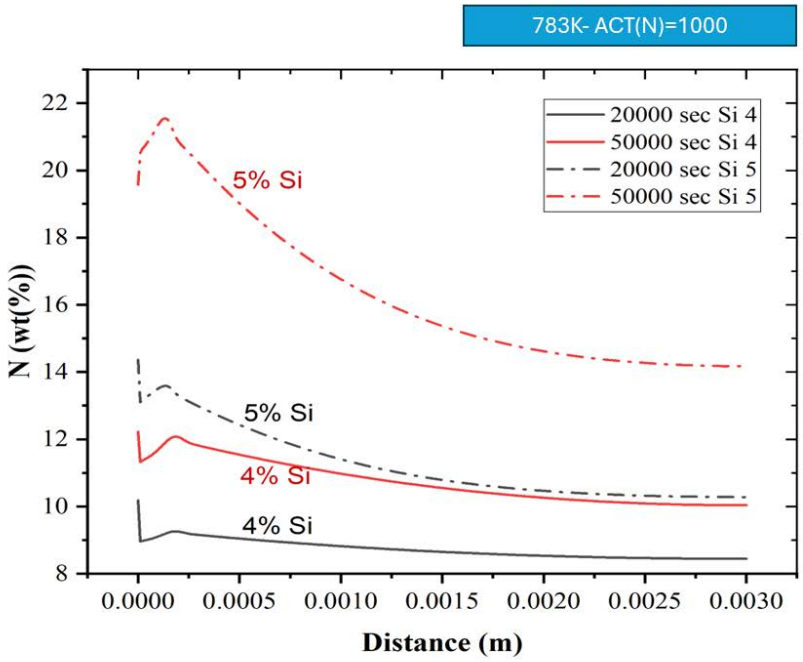

Figure 4.6. 2: Comparison of Nwt%/ distance graph for 4wt% Si and 5.16wt%Si [20000s &50000s]

Therefore, the formation of γ' occurs faster as well, creating the desired hardened surface, thick in γ'nitrides. This is also confirmed by looking at ***Figure 4.6. 1*** and comparing to ***Figure 4.4. 4***. For higher Si content (5.16wt%), at 20000s the amount of γ' nitrides at the beginning of the region reaches **12.1wt%**, while on the on the other hand, for the simulation with the lower Si content (4wt%), at a higher point in time, 50000s, the γ'-nitride amount is lower, at **7.9wt%.** Finally, based on ***Figure 4.6. 3***, at the end of the simulation (500000s), the percentage of γ'-nitrides formed at the start of the region is **30%** and the phase reaches deeper into the region, at **distance 4.7e-4**, before it stops forming, creating a thick nitride layer. A comparison between the amount of γ'-nitrides formed for the two Si contents is exhibited in ***Figure 4.6. 4***.

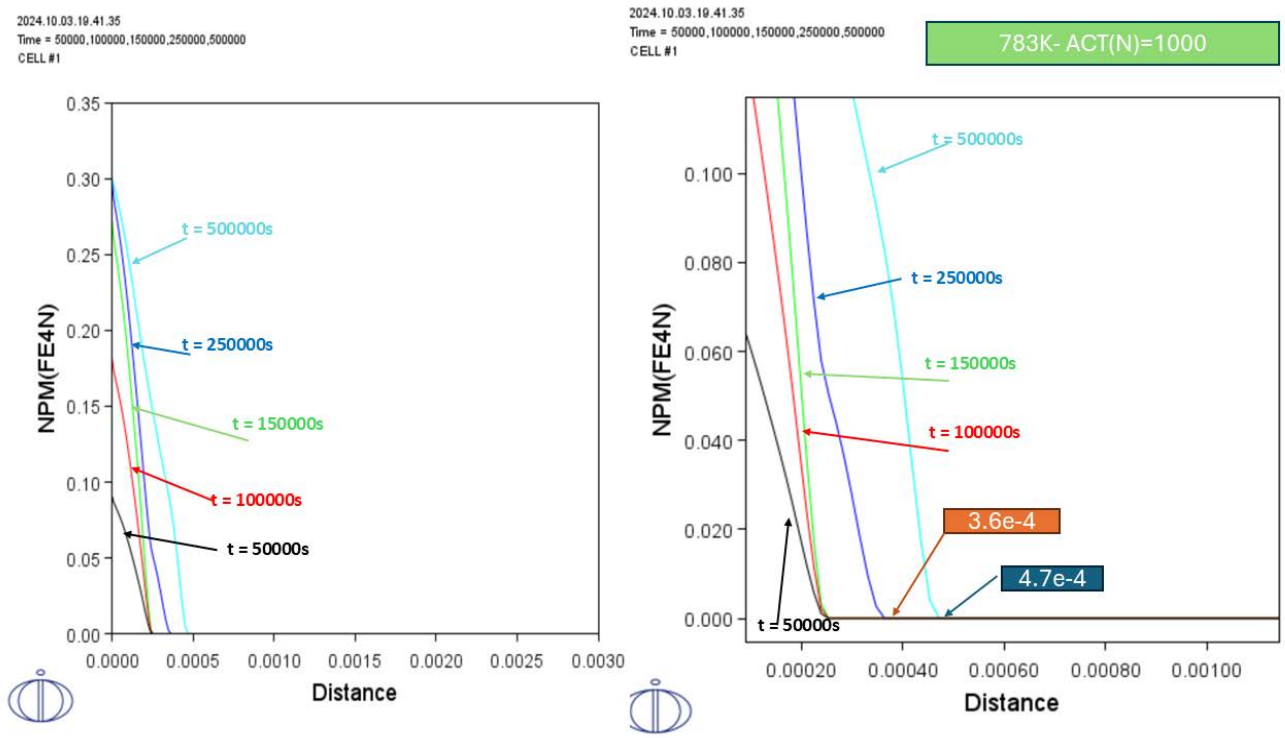

Figure 4.6. 3: Amount of γ' (x-axis) / Distance into the surface (y-axis) [ACT(N)=1000] [510◦C]

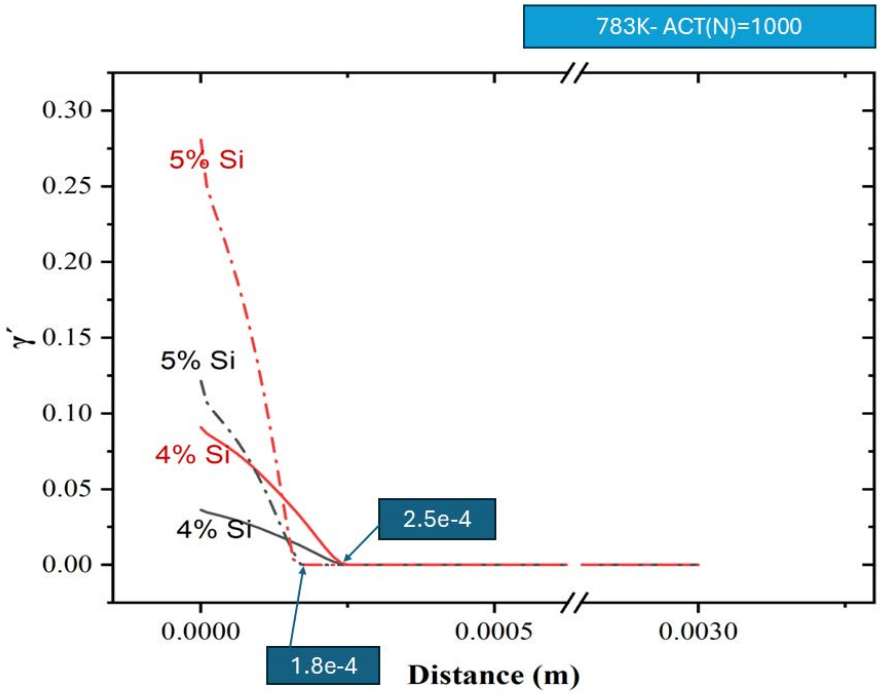

Figure 4.6. 4: Comparison of γ'/ distance graph for 4wt% Si and 5.16wt%Si [20000s &50000s]

CHAPTER 6: CONCLUSIONS

1. The t**hermodynamic** calculations lead to the following conclusions:
   - The suspension of Si_3N_4 causes much higher percentages of ε formation, however a lot less γ'. Additionally, the γ'-nitrides are restricted to lower nitrogen percentages and to a smaller region.
   - The addition of Al causes the introduction of κ-phase for low nitrogen percentages. The increase of Al content causes slight decrease in γ'-nitrides, however, leads to formation at higher N percentages.

2. In the attempt to perform the nitriding kinetic simulation for a region inside the compound layer (including ε-nitrides), the results of the calculations did not exhibit logical meaning and, therefore, were incorrect. That is why part of the **diffusion zone** was then selected for the simulations for this thesis.

3. Conclusions concerning the **effect of nitrogen activity** on cast iron nitriding simulation:
   - For higher N activity the formation of γ' nitrides are enhanced and are formed in a more stable manner and at higher percentage into the material's surface.
   - Higher N activity causes nitrogen to penetrate deeper into the material over a given period, resulting in a thicker γ'-nitride layer.
   - Nitrogen activity is a controllable factor which can be set at a specific value in order to favor the formation of the appropriate nitrides in order to achieve the desired material properties. Higher nitrogen activity levels favor the formation of γ'-nitrides (Fe_4N) which contribute to increased surface hardness of the cast iron.

4. Conclusions concerning the **effect of temperature increase** [510◦C to 520◦C] on cast iron nitriding simulation:
   - The 10-degree temperature increase results in the diffusion of higher nitrogen percentages, at greater distance into the region.
   - Simulations for 10-degree higher temperature also exhibit the formation of γ'-nitrides taking place even deeper into the diffusion zone, creating a thicker nitride layer.
   - Finally, with the temperature increase, the final γ'-nitride layer into the region is noted to be less rich in nitrides.

5. Conclusions concerning the **effect of Si** alloying content on cast iron nitriding simulation:
   - Higher content of Si alloying element causes faster Nitrogen diffusion into the region of the diffusion zone, therefore higher nitrogen percentages are reached sooner at deeper distances.
   - Higher content of Si alloying element leads to larger amounts of γ'-nitrides to be formed faster, however creating a less thick nitride layer into the diffusion zone, but richer in γ'-nitride quantities.

CHAPTER 5: REFERENCES

[1] O. Celik, H. Ahlatci, E.S. Kayali, H. Cimenoglu, High temperature abrasive wear behavior of an as-cast ductile iron, Wear 258 (2005) 189–193. https://doi.org/10.1016/j.wear.2004.09.004.

[2] M.A.J. Somers, Development of Compound Layer and Diffusion Zone during Nitriding and Nitrocarburizing of Iron and Steels, in: Compr. Mater. Process., Elsevier, 2014: pp. 413–437. https://doi.org/10.1016/B978-0-08-096532-1.01215-2.

[3] E. Kondakci, N. Solak, The Effect of Microstructure on Nitriding Mechanism of Cast Iron, Int. J. Met. 14 (2020) 1033–1040. https://doi.org/10.1007/s40962-019-00404-2.

[4] G.N. Haidemenopoulos, Physical Metallurgy: Principles and Design, 1st ed., CRC Press, 2018. https://doi.org/10.1201/9781315211220.

[5] H. Du, M.A.J. Somers, Microstructural and compositional evolution of compound layers during gaseous nitrocarburizing, (n.d.).

[6] J.-Q. Sun, Z.-F. Yan, H.-Z. Cui, J. Li, J.-S. Wang, Y.-B. Chen, Surface catalysis gaseous nitriding of alloy cast iron at lower temperature, Catal. Today 158 (2010) 205–208. https://doi.org/10.1016/j.cattod.2010.03.028.

[7] M. Ekström, S. Jonsson, High-temperature mechanical- and fatigue properties of cast alloys intended for use in exhaust manifolds, Mater. Sci. Eng. A 616 (2014) 78–87. https://doi.org/10.1016/j.msea.2014.08.014.

[8] G.A. Çelik, M.-I.T. Tzini, Ş. Polat, Ş.H. Atapek, G.N. Haidemenopoulos, Thermal and microstructural characterization of a novel ductile cast iron modified by aluminum addition, Int. J. Miner. Metall. Mater. 27 (2020) 190–199. https://doi.org/10.1007/s12613-019-1876-8.

[9] J. Wahyuadi, T. Soemardi, B. Suharno, R. Sulamet-Ariobimo, Effects of Carbon Equivalent on the Microstructures of Thin Wall Ductile Iron, 5 (2011) 266–270.

[10] G.E. Totten, ed., Steel Heat Treatment: Metallurgy and Technologies, 0 ed., CRC Press, 2006. https://doi.org/10.1201/NOF0849384523.

[11] Steels, Elsevier, 2006. https://doi.org/10.1016/B978-0-7506-8084-4.X5000-6.

[12] M. Ahmed, M. Soliman, M. Youssef, R. Bähr, A. Nofal, Effect of Niobium on the Microstructure and Mechanical Properties of Alloyed Ductile Irons and Austempered Ductile Irons, Metals 11 (2021) 703. https://doi.org/10.3390/met11050703.

[13] D. Zeng, Y. Zhang, J. Liu, H. He, X. Hong, Characterization of titanium-containing compounds in gray iron, Tsinghua Sci. Technol. 13 (2008) 127–131. https://doi.org/10.1016/S1007-0214(08)70022-1.

[14] E. T, H. J, Influence of Al and Ti on microstructure and quality of compacted graphite iron castings, Metalurgija 48 (2009).

[15] M. Górny, M. Kawalec, Effects of Titanium Addition on Microstructure and Mechanical Properties of Thin-Walled Compacted Graphite Iron Castings, J. Mater. Eng. Perform. 22 (2013) 1519–1524. https://doi.org/10.1007/s11665-012-0432-8.

[16] M. Górny, M. Kawalec, Role of Titanium in Thin Wall Vermicular Graphite Iron Castings Production, Arch. Foundry Eng. 13 (2013) 25–28. https://doi.org/10.2478/afe-2013-0030.

[17] D. Holmgren, A. Diószegi, I.L. Svensson, Effects of nodularity on thermal conductivity of cast iron, Int. J. Cast Met. Res. 20 (2007) 30–40. https://doi.org/10.1179/136404607X202690.

[18] C.A. Cooper, R. Elliott, R.J. Young, Investigation of elastic property relationships for flake and spheroidal cast irons using Raman spectroscopy, Acta Mater. 50 (2002) 4037–4046. https://doi.org/10.1016/S1359-6454(02)00202-1.

[19] H. Nakae, H. Shin, Effect of Graphite Morphology on Tensile Properties of Flake Graphite Cast Iron, Mater. Trans. 42 (2001) 1428–1434. https://doi.org/10.2320/matertrans.42.1428.
[20] M.M. Ibrahim, A. Nofal, M.M. Mourad, Microstructure and Hot Oxidation Resistance of SiMo Ductile Cast Irons Containing Si-Mo-Al, Metall. Mater. Trans. B 48 (2017) 1149–1157. https://doi.org/10.1007/s11663-016-0871-y.